PHILOSOPHICAL TRANSACTIONS OF THE ROYAL SOCIETY B BIOLOGICAL SCIENCES

Flow Behaviour of Blood Cells and Rigid Spheres in an Annular Vortex

T. Karino and H. L. Goldsmith

Phil. Trans. R. Soc. Lond. B 1977 **279**, 413-445
doi: 10.1098/rstb.1977.0095

FLOW BEHAVIOUR OF BLOOD CELLS AND RIGID SPHERES IN AN ANNULAR VORTEX

By T. KARINO and H. L. GOLDSMITH
McGill University Medical Clinic, Montreal General Hospital, Montreal, Quebec, Canada

(*Communicated by F. C. MacIntosh, F.R.S.* – *Received* 26 *July* 1976)

[Plate 1]

CONTENTS

Vol. 279. B 967. 35 [Published 10 June 1977

The behaviour of human and frog red cells, platelets and rigid spheres were studied in the annular vortex formed in steady or pulsatile flow at the sudden concentric expansion of a 151 μm into 504 μm diameter glass tube. During a single orbit the measured particle velocities and paths in steady flow were in good agreement with those calculated for the fluid, predicted by theory to circulate in closed orbits. Over longer periods, however, single blood cells and latex spheres < 20 μm diameter migrated across the streamlines out of the vortex at a rate depending on the Reynolds number whereas spheres and aggregates of red cells > 30 μm diameter remained in the vortex at all Reynolds numbers. Similar behaviour was noted in pulsatile flow when the vortex moved in phase with upstream fluid velocity and particles described spiral orbits of continually changing diameter. With red cell suspensions of 15–45 % haematocrit in steady flow, migration of the corpuscles was also observed and resulted in the formation of a particle-free vortex. In pulsatile flow, cells were always present in the vortex, but their concentration which varied periodically was lower than that in the mainstream. The formation of aggregates of latex spheres and human platelets through collisions occurring in orbit, and their migration to the vortex centre was also observed.

Nomenclature

a, c	constants
b	radius of rigid sphere
B	amplitude of oscillatory pressure gradient
B_0	$= 8\eta_0 Q_0/\pi R^4$
D_1, D_2	respective diameters of inner and outer tubes of the sudden expansion
f	frequency of oscillatory flow
G, G_{rz}	shear rate, component of shearing rate of strain
H	step height $= \frac{1}{2}(D_2 - D_1)$
L; $L_{\min}$, $L_{\max}$	axial distance of reattachment point from origin of the expansion; minimum and maximum values in pulsatile flow
M'_0, M'_{10}	function of α and r/R, function of α in oscillatory flow
Q_0	steady volume flow rate
Q^*	amplitude of oscillatory volume flow rate
r, Z, θ	cylindrical polar coordinates
r_0	radial distance of vortex centre from tube axis
r_e	equivalent ellipsoidal axis ratio
R	tube radius
Re, Re_p	tube Reynolds number $= \bar{U}D\rho_0/\eta_0$, particle Reynolds number $= U_M b\rho_0/\eta_0$
t	time

T_0, T_c	period to circulate around orbit, period of rotation of blood cell
u, w; U, W	respective particle velocities in the Z- and r-direction; respective fluid velocities
U_M	maximum fluid velocity in the backflow region of the vortex
$\bar{U}$	mean upstream fluid velocity
v; V	particle linear velocity $= \sqrt{(u^2+w^2)}$; fluid linear velocity
ΔV	volume displacement per half cycle in oscillatory flow
y, y_M; y^*	distance from tube wall $= R-r$, value at $U = U_M$; equilibrium value of y
X, Y, Z	Cartesian coordinate axes
Y_0, Z_0	respective radial and axial location of vortex centre
α	Womersley parameter $= R(\omega\rho_0/\eta_0)^{\frac{1}{2}}$
β	$= y/y_M$
$\epsilon_0(\alpha, r/R)$	phase angle in oscillatory flow
ζ'_θ; ζ	vorticity $= (\partial W/\partial z - \partial U/\partial r)$; dimensionless vorticity $= \zeta'_\theta D_1/\bar{U}$
η_0	viscosity of suspending phase
ρ_0, ρ	density of suspending phase and particle respectively
τ, $\bar{\tau}$	particle residence time, mean value
ψ', ψ	stream function, dimensionless stream function $= \psi'/D_1^2\bar{U}$
ω	angular velocity of oscillatory flow
Ω	angular velocity of rigid-body motion
ϕ, ϕ'	orientation of cell axis of revolution with respect to the r-axis, orientation with respect to the normal to the streamline

1. Introduction

During the last ten years there have been a number of theoretical and experimental studies of the flow field downstream of constrictions in tubes (Forrester & Young 1970*a*, *b*; Lee & Fung 1971; Golia & Evans 1973), and of laminar sudden expansions in plane (Hung & Macagno 1966; Durst, Melling & Whitelaw 1972, 1974),and axisymmetric flow (Macagno & Hung 1967; Back & Roschke 1972; Iribarne, Frantisak, Hummel & Smith 1972; Feuerstein, Pike & Round 1975). The experimental work was conducted in channels and tubes having diameters from 2 to 25 mm, and the streamlines and dimensions of the eddies in the region of flow separation were obtained with the aid of flow visualization techniques such as the injection of dye into the fluid or the addition of small tracer particles. Velocity distributions in an abrupt expansion have also been measured using laser anemometry in the case of air flow (Durst *et al.* 1972, 1974) and high speed cine photography with suspensions of polystyrene spheres in aqueous glycerol (Feuerstein *et al.* 1975). The dispersed particles here, and in other of the above mentioned studies, served essentially to act as tracers for the fluid streamlines.

The present paper is concerned with the motions of particles suspended in viscous fluids within a captive annular vortex formed at an abrupt tubular expansion, for which a method of computing the fluid streamlines and vorticity contours has been given (Macagno & Hung 1967). The effects of fluid inertia and of the vessel walls on the particle movements were considered to be of particular interest, as were the interactions occurring between particles in the vortex. The work was motivated by our interest in the flow behaviour of blood corpuscles at sites of flow separation in mammalian arteries where early atherosclerotic changes in the vessel wall occur (Fox & Hugh 1966; Caro, Fitz-Gerald & Schroter 1971), and where there is evidence

PHILOSOPHICAL TRANSACTIONS OF THE ROYAL SOCIETY B BIOLOGICAL SCIENCES

that platelet aggregates (thrombi) accumulate and are deposited onto the wall, a phenomenon of some importance in understanding the development of vascular occlusions (Packham, Rowsell, Jørgensen & Mustard 1967). Among such sites are the not uncommon constrictions (stenoses) in arteries for which the abrupt tubular expansion serves as an idealized model. Indeed, *in vitro* studies using constrictions and abrupt expansions (Benis *et al.* 1975; Blackshear *et al.* 1971; Smith, Blick, Coulson & Stein 1972; Stein & Sabbah 1974) as well as *in vivo* studies with implanted orifice rings (Gott *et al.* 1969; Foster & Dobell 1971) have demonstrated that platelet thrombus formation and adhesion to the wall occurs in the region of the eddy. Unfortunately, such experiments have served more to test the compatibility of biomaterials on the surface of the flow channel to blood than to study the relation between the flow regime and platelet aggregation.

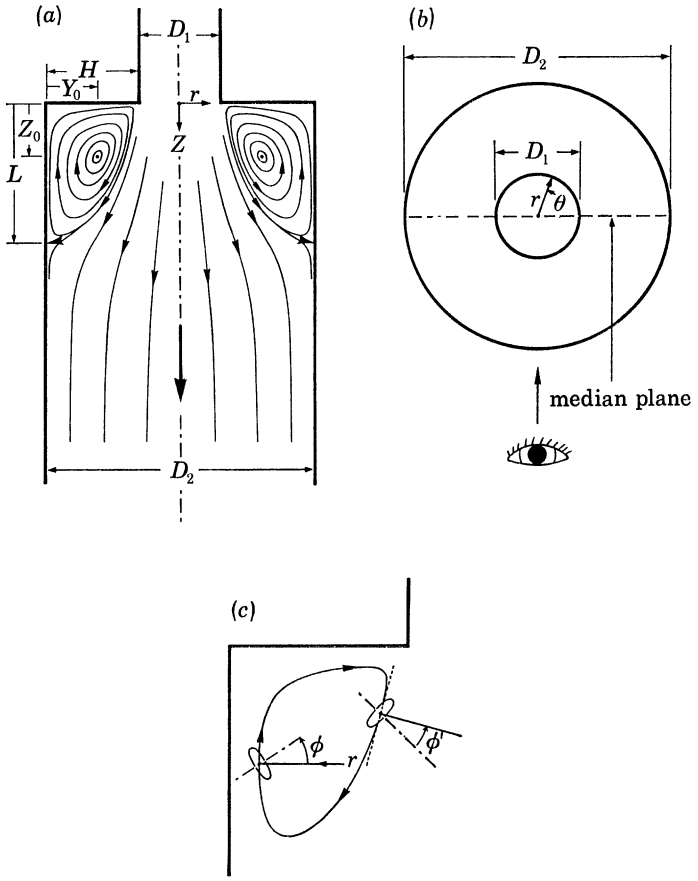

FIGURE 1. Schematic drawing of the expansion and coordinate systems. (*a*) Common median plane of the two tubes showing the coordinates r, Z of the flow field with origin at the entry of the expansion, and the location Y_0, Z_0 of the vortex centre and the reattachment point (L). (*b*) End on view of the expansion with cylindrical polar coordinates r and θ. (*c*) Orientation of the projection of the particle axis of revolution (dashed line) in the median plane with respect to the r-axis (ϕ) and the normal to the tangent of the streamline (ϕ').

Based on theoretical and experimental studies of the flow of Newtonian fluids through constrictions and abrupt expansions, there has also been speculation about the effects of the vortex flow field on diffusive and convective transport of dissolved substances such as lipoproteins and oxygen in the plasma to and from the vessel wall (Caro *et al.* 1971; Caro & Nerem 1973; Back 1975*a*, *b*). Changes in the normal environment of the artery wall brought about by flow

disturbances may in turn lead to alterations in the vessel wall which favour the adhesion of platelets (Caro *et al.* 1971) and may even mechanically weaken it, resulting in the development of a post-stenotic dilatation (Roach 1972).

Nevertheless, the main participants in the formation of a thrombus are the blood corpuscles, and with this in mind we thought it appropriate to make observations of their flow behaviour in an annular vortex. To this end, expansions of small dimensions were constructed using tubes of 151 and 504 μm diameter, and the suspensions of the 2–20 μm diameter corpuscles were viewed through a microscope. The work involved the use of microrheological techniques (Goldsmith & Mason 1975), previously described in studies of the flow behaviour of human red blood cells and platelets in rigid, straight tubes (Goldsmith & Marlow 1972; Frojmovic, Newton & Goldsmith 1976) as well as in the vortex formed downstream of an asymmetric spherical obstruction in a tube (Yu & Goldsmith 1973).

Preliminary results had shown (Goldsmith 1974) that while single red blood cells travelled outward across the streamlines of the annular vortex and rejoined the mainstream, aggregates migrated into equilibrium orbits or the vortex centre, and remained there at all Reynolds numbers. Similarly, recent work by Morton, Parmentier & Petschek (1975), using a stagnation point flow chamber surrounded by a forward facing step, has shown that in dog blood, platelet aggregates form and grow in the vortex situated at the corner of the step (Moffatt 1964), at the same time that many red cells migrate out.

The present work extends the preliminary observations to a detailed study of the paths and orientations of human and frog blood corpuscles, and of the flow behaviour of 2.6–50 μm diameter latex spheres. The particles were observed and photographed in the common median, rZ-plane of the expansion, as shown schematically in figure 1. The lateral (Y_0) and axial (Z_0) positions of the vortex centre and the vortex length L were also determined. Measurements were made in steady, as well as in pulsatile flow, i.e. oscillatory, superimposed on steady flow. The results have substantiated the existence of a particle migration phenomenon, earlier found, which is both size and Reynolds number dependent, and which appears to provide a mechanism whereby aggregates of blood cells formed in the vortex can accumulate and grow in size.

2. Experimental

(*a*) *Apparatus*

(i) *Flow tubes and infusion pumps*

Abrupt expansions were constructed by tightly and concentrically fitting thick-walled small diameter tubes, cut accurately at right angles, into larger diameter thin-walled glass tubes. For the work with latex spheres and blood cells, the expansions were made by using precision bore glass tubes of 151 and 504 μm diameter respectively. A 10 mm section of the smaller tube was inserted into the ends of two pieces of the larger tube; a small quantity of epoxy cement was applied to the gap between the outer tubes which were then pushed together to provide a seal. For the experiments with the larger carbon spheres, expansions consisting of a 0.5 mm diameter stainless steel or brass tube fitting tightly into a 3.0 mm precision bore glass tube were constructed.

The expansions were mounted on microscope slides and to minimize optical distortion, surrounded by chambers filled with a liquid of the same refractive index as that of the suspending phase (Goldsmith & Marlow 1972; Yu & Goldsmith 1973). The slides in turn were clamped

onto a moveable and vertically mounted platform which could be driven at continuously variable speeds from 0.01 to 20 mm s^{-1} in the direction of flow by means of an electronically controlled d.c. motor via a gear box (Goldsmith & Marlow 1972). Both ends of the flow tubes fitted snugly into short lengths of polyethylene tubing through which they were connected to two reservoirs, at the upper end to a 3 or 5 ml syringe via a 20 mm length of 17-gauge steel needle, at the lower end to a reservoir open to the atmosphere.

An infusion-withdrawal pump attached to the moveable platform drove the syringe plunger at continuously variable speeds covering a range of volume flow rates from 10^{-4} to 10^{-2} ml s^{-1} and the suspension thus flowed up or down the tube from one reservoir to the other to produce a steady expansion or convergent flow depending on the purpose of the experiments.

Pulsatile flow was obtained by superimposing a sinusoidal oscillatory flow in parallel with a steady flow. The oscillatory flow was produced by a reciprocating pump consisting of a 25 µl precision bore syringe whose plunger was driven in simple harmonic motion by a crank-shaft mechanism attached to a flywheel rotated by a continuously variable, electronically controlled, d.c. motor drive at speeds from 3 to 195 rev/min. The displacement volume, ΔV, per half cycle could be varied by changing the distance of the crank arm from the centre of the flywheel. A contactor attached to the flywheel of the reciprocating pump activated a timing light within the camera marking the film at 0° and 180° within each cycle. The steady volume flow rate was determined by weighing the suspension expelled in a given time.

(ii) *Optical system and camera*

As previously described (Yu & Goldsmith 1973) the events occurring in the tube were photographed through the microscope at nominal magnifications of × 12.5 to × 200 using a 400 ft Locam 16 mm cine camera at film speeds from 50 to 500 pictures/s, and a 400 ft Hycam 16 mm camera at speeds from 500 to 3000 pictures/s. A beam splitter attached to the camera and positioned close to the microscope eyepiece, but not making contact, enabled simultaneous observations of the events in the tube to be made while filming. A 35 mm camera (Zeiss Ikon Icarex) was also used to photograph the flow patterns in blood undergoing steady flow.

Illumination was provided by a Reichert Binolux twin-lamp assembly supplying either low-intensity light from a tungsten filament lamp, or high intensity light from a 200 W d.c. mercury arc lamp with a filter to eliminate ultraviolet illumination. Besides bright-field illumination, dark-field illumination giving intense, clear images of the paths of the tracer particles was also used for experiments in which observations were made over long periods of time.

Kodak Double X negative films were used with a 1/9 rotating shutter synchronized with the film transport in the camera. The films were subsequently projected onto a drafting table and analysed frame by frame with the aid of a Photo-Optical Data stop-motion 16 mm movie projector (Model 224-A, L-W Photo Inc., Van Nuys, Calif.).

(*b*) *Suspensions*

The suspensions used and their physical properties at the laboratory temperature of 22 ± 0.5 °C are listed in table 1.

(i) *Human hardened red blood cells* (*h.b.c.*)

Hardened cells (ρ = 1.13 g ml^{-1}) were prepared as previously described (Yu & Goldsmith 1973) and suspensions having the desired particle-fluid density differences were made up using water and aqueous cadmium-nitrate solutions.

(ii) *Humam normal red cells (r.b.c.) and platelet-rich plasma (p.r.p.)*

Fresh blood was drawn from healthy donors by venipuncture into a sterilized plastic syringe containing 3.8 % sodium-citrate, 1 part to 9 parts of blood, or 2–5 units heparin per ml blood. The collected blood was gently mixed and allowed to stand for 30 min in a constant temperature bath at 37 °C before centrifuging at 80 *g* for 15 min at room temperature and drawing off the supernatant p.r.p. Dilute red cell suspensions and blood at haematocrits from 15 to 30 % were prepared by resuspending packed red cells in platelet-poor plasma. Whole blood at haematocrits from 15 to 30 % were prepared by resuspending packed red cells in platelet-poor plasma. Whole blood at a haematocrit of 45 % was also used.

TABLE 1. PHYSICAL PROPERTIES OF SUSPENSIONS AT 22 ± 0.5 °C

	suspended phase			suspending phase		
ystem	particle	mean diameter / μm	density, ρ / g ml^{-1}	fluid	viscosity, η_0 / Pa s	$\Delta\rho = \rho - \rho_0$ / g ml^{-1}
1	hardened human red cells (h.b.c.)	7.5	1.13	water	0.0010	+0.13
2	h.b.c.			15–20 % aqueous $Cd(NO_3)_2$	0.0011 to 0.0012	−0.06 to 0
3	normal human red cells (r.b.c.)	8.2	1.10	plasma	0.002	+0.080
4	human platelets	3.6	1.05	plasma	0.002	+0.030
5	frog red cells†	12.5 × 21.6	—	frog Ringer solution	0.0010	> 0
6	carbon microspheres‡	13.0, 30.3	1.39	76% ethylene glycol, 8.5% benzyl alcohol, 15.5% tetrabromo-ethane	0.0156	0
7	polystyrene latex§ spheres	2.6, 9.8, 20.0, 32.0, 50.0	1.06	25% aqueous glycerol	0.0019	0

† Particle shape approximates that of a biconvex ellipsoid, maximum thickness = 3.7 μm.
‡ 3 M Company.
§ Particle Information Services, Grants Pass, Oregon.

(iii) *Frog red cells*

10 ml of heparinized, freshly drawn bullfrog blood was centrifuged at 2000 *g* for 15 min and the red cells separated from the plasma. Dilute suspensions were prepared by resuspending 0.2 ml of packed frog red cells in 15 ml of a mixture of 1 vol. of plasma and 3 vol. of frog Ringer solution.

(iv) *Rigid spheres*

Neutrally buoyant suspensions of carbon microspheres (ρ = 1.39 g ml^{-1}) with mean diameters of 13.0 and 30.3 μm, and highly monodisperse polystyrene latex spheres (ρ = 1.06 g ml^{-1}) having diameters from 2.6 to 50 μm were used. In the case of the carbon microspheres the refractive index of the suspending mixture of oils (system 6) matched that of the glass tube (n_D = 1.474), thereby avoiding all optical distortion.

(*c*) *Physical properties of the suspensions*

Fluid densities were measured by using pycnometers. Mean densities of the model particles were determined by measuring the densities of the suspending fluids in which almost zero

sedimentation of particles occurred under a centrifugal force of *ca.* 4000 *g*. The densities of the h.b.c. and r.b.c. were determined as previously described (Yu & Goldsmith 1973). The viscosities of the suspending fluids and that of blood were measured by using a Cannon-Ubbelohde capillary viscometer and a Brookfield cone and plate microviscometer respectively. Except for the experiments with blood at haematocrits $\geqslant$ 15 %, concentrations of particles in the suspensions were less than 1 % by volume.

3. Results

(*a*) *Steady flow*

(i) *General observations*

The paths and orientations of h.b.c. (system 1) within the vortex were determined at tube Reynolds numbers *Re*, based on upstream mean fluid velocity $\bar{U}$ and tube diameter D_1, from 0 to 75. As predicted by the theory (Macagno & Hung 1967) even at $Re < 1$ a small annular vortex was observed at the very corner of the expansion. As $\bar{U}$ increased, a triangular-shaped vortex of progressively increasing length developed. Examples of the paths and orientations

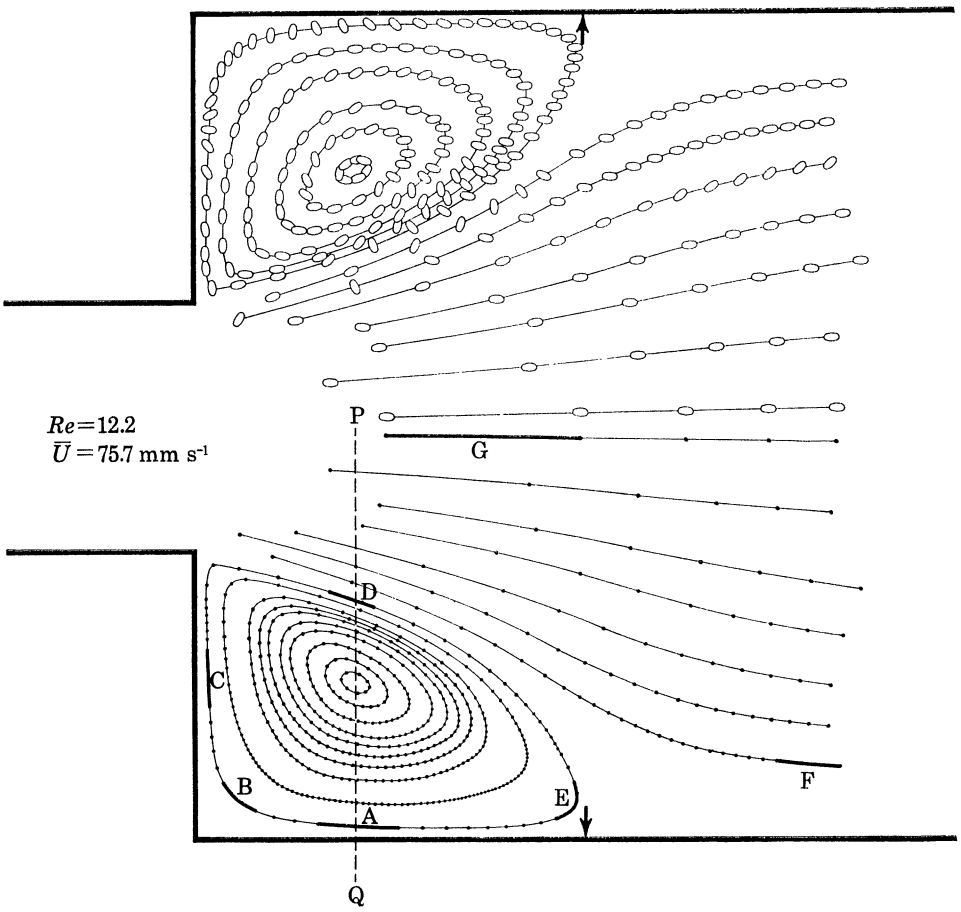

Figure 2. Single orbits of glutaraldehyde-hardened human red blood cells in the median plane of the annular vortex formed downstream of the expansion of a 151 μm into a 504 μm tube at $Re = 12.2$. The orientation of the cells are drawn on the orbits in the upper portion of the diagram. The arrows indicate the reattachment point, $L = 230$ μm. The letters A–G and O indicate the positions at which particle velocities were measured and are listed in table 2.

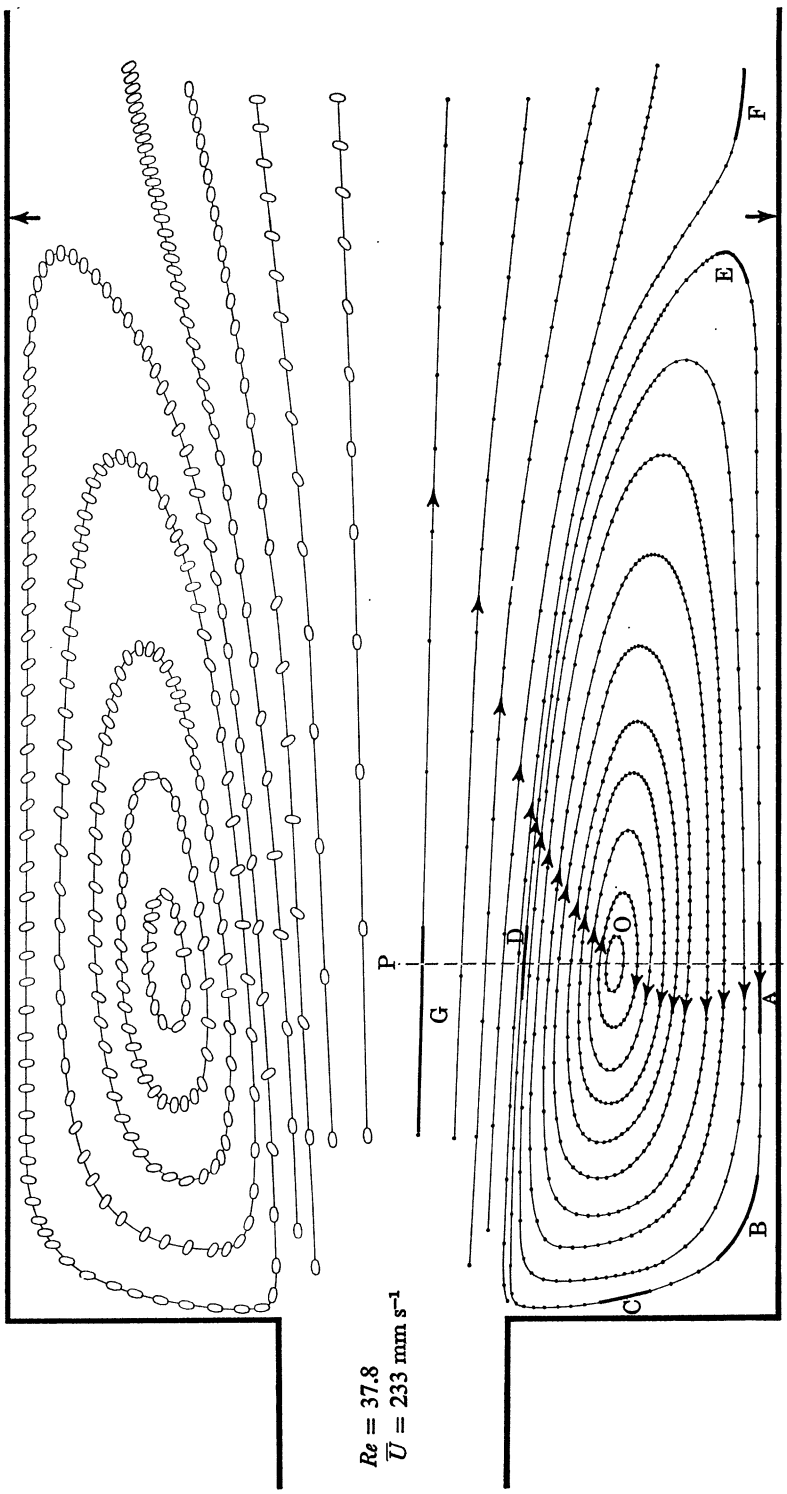

FIGURE 3. Orbits and orientations of human h.b.c. as in figure 2 at a higher $Re = 37.8$; $L = 715$ μm.

PHILOSOPHICAL TRANSACTIONS OF THE ROYAL SOCIETY B BIOLOGICAL SCIENCES

followed by the h.b.c. during a single orbit are given in figures 2 and 3 at $Re = 12.2$ and 37.8 respectively. At the lower Re, and in the almost circular orbits close to the vortex centre, the cells travelled with virtually constant linear velocities, while in the outer, more elliptical orbits the velocities varied considerably, being high in the forward flowing portion of the vortex, low in the reverse flow region, and remaining low until forward motion was resumed.

Most striking of all, was the observation made with human blood cells in systems 1–4, as well as with the latex spheres $\leqslant 20$ μm diameter in system 7 that, over several orbits, the particles could be seen to migrate spirally outward across the closed fluid streamlines and after many orbits rejoined the mainstream. Thus, after a certain time, the vortex emptied of particles, the rate of migration depending on particle size and Reynolds number, as detailed below. First, however, the characteristics of the vortex and the orientations of blood cells within the orbits will be described.

TABLE 2. PARTICLE TRANSLATIONAL VELOCITIES $|v|$ IN VARIOUS REGIONS OF THE VORTEX, SYSTEM 1

location†	$\lvert v\rvert$/(mm s^{-1})	
	$Re = 12.2$	$Re = 37.8$
O	0.54	2.44
A	0.64	3.59
B	0.36	3.03
C	1.46	6.93
D	11.8	94.1
E	0.30	0.84
F	3.30	0.95
G	48.6	272

† As indicated on figures 2 ($Re = 12.2$) and 3 ($Re = 37.8$).

TABLE 3. ORBIT TIMES AND MEAN VELOCITIES OF h.b.c. IN THE VORTEX, SYSTEM 1

orbit†	orbit time, T_o/s		mean velocity/(mm s^{-1})	
	$Re = 12.2$	$Re = 37.8$	$Re = 12.2$	$Re = 37.8$
1	0.091	0.034	0.53	2.44
2	0.094	0.035	1.17	5.59
3	0.094	0.036	1.89	9.46
4	0.099	0.037	2.46	12.7
5	0.103	0.039	2.73	15.1
6	0.121	0.043	2.71	17.6
7	0.131	0.051	2.78	18.6
8	0.155	0.064	2.66	17.5
9	0.251	0.103	2.09	12.8
10	0.704	0.311	0.92	4.89

† The orbits are numbered starting at the centre of the vortex and are those shown in the lower halves of figures 2 and 3.

(ii) *Velocity distribution*

Particle linear velocities, v, were obtained from the times to pass over short segments of known length within an orbit. Table 2 gives values of $|v|$ at the particular positions in the vortex labelled in figures 2 and 3. The times to execute one orbit as well as the mean translational velocity within the orbit (calculated from the measured orbit contour) are given in table 3 for the ten orbits drawn in figures 2 and 3. It is evident that close to the vortex centre, the

orbit times were almost constant (the first 3 orbits drawn in figures 2 and 3). Thus, at the lower *Re*, motion in the circular innermost orbits approximated flow inside a rotating cylinder in which the fluid elements undergo rigid-body motion with constant angular velocity. With increasing orbit number, however, the mean particle velocities increased and reached a maximum in that orbit in which the backflow velocity was a maximum (cf. figures 6*a* and 6*b*), and then decreased again.

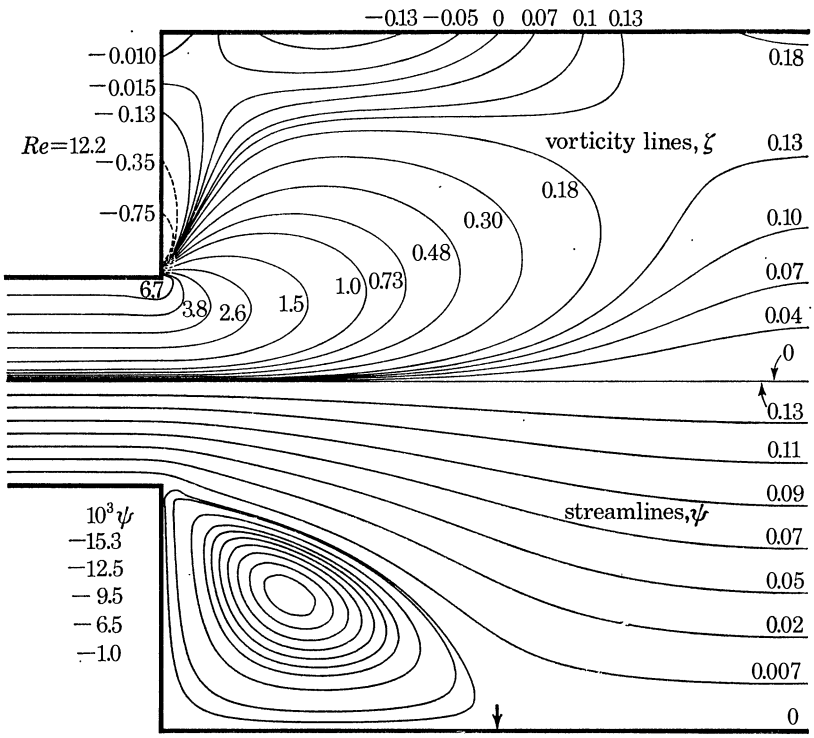

FIGURE 4. Dimensionless vorticity contours and streamlines calculated from theory (Macagno & Hung 1967) for flow at $Re = 12.2$ corresponding to the conditions prevailing in figure 2. The values of ψ on the lower left list the stream function from the centre to the periphery of the vortex on alternate streamlines.

The above results were compared with theory based on the computations of Macagno & Hung (1967).† Dimensionless stream functions and vorticities defined by

$$\psi = \psi'/D_1^2\bar{U}, \quad \zeta = \zeta'_\theta D_1/\bar{U}, \tag{1}$$

where ψ' is the stream function and ζ'_θ $(= \partial W/\partial z - \partial U/\partial r)$, the only non-zero component in vorticity, were calculated at the two *Re* which obtained in figures 2 and 3, and are shown in figures 4 and 5. A comparison of the measured and calculated streamlines in figures 2–5 indicates qualitatively good agreement between theory and experiment. The location of the reattachment point, L, and the location Z_0, Y_0 of the vortex centre (figure 1*a*) were within 5% of those theoretically predicted. In addition, as illustrated in figures 6*a* and 6*b*, the measured particle translational velocities, v, at points lying on the line PQ passing through the vortex centre and normal to the tube wall (figures 2 and 3) were in excellent agreement with those of

† The authors are indebted to Dr T.-K. Hung (University of Pittsburgh) who kindly provided data on stream functions and vorticities in the annular vortices corresponding to the conditions of the above experiments.

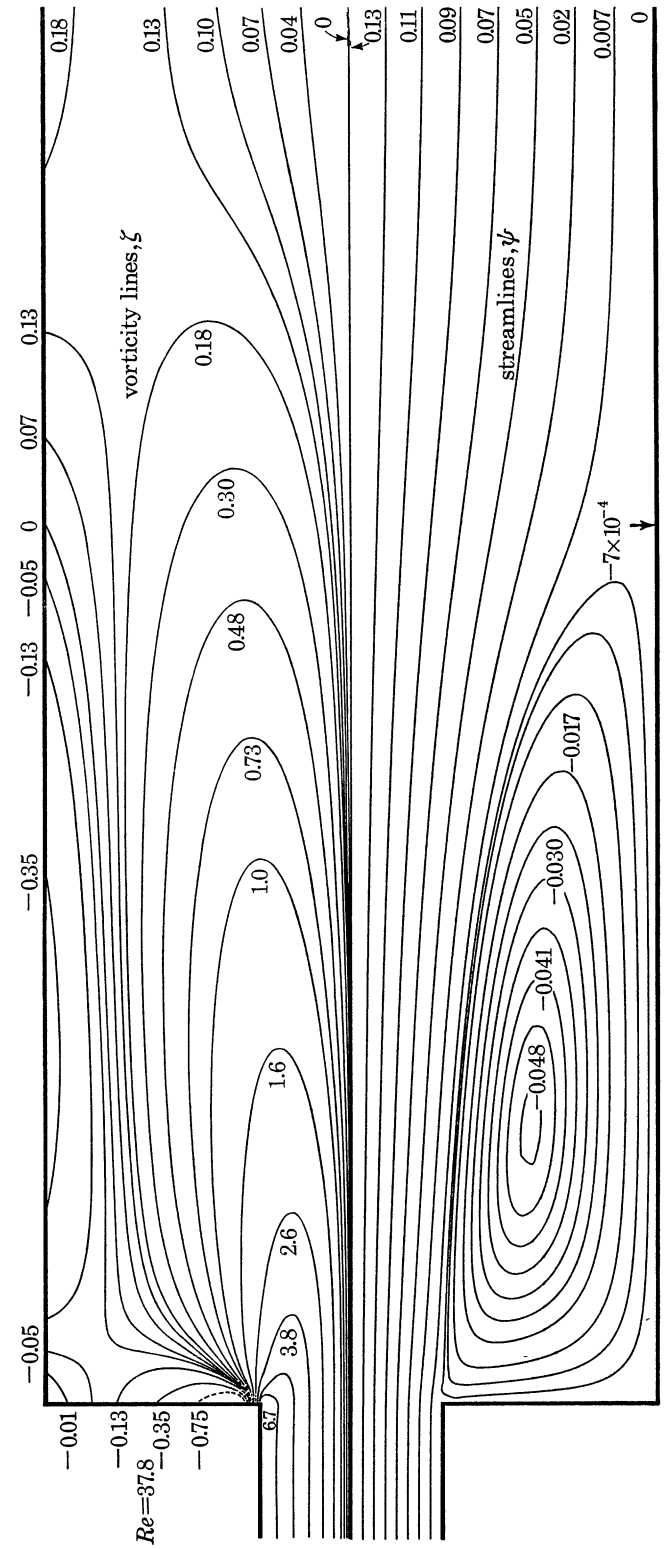

FIGURE 5. Calculated vorticity contours and streamlines for $Re = 37.8$ corresponding to the vortex shown in figure 3.

PHILOSOPHICAL TRANSACTIONS OF THE ROYAL SOCIETY B BIOLOGICAL SCIENCES

the fluid, V, calculated from theory (Macagno & Hung 1967) using the computed stream functions ψ':

$$U = -\frac{1}{r}\frac{\partial \psi'}{\partial r}, \quad W = \frac{1}{r}\frac{\partial \psi'}{\partial z}, \tag{2a}$$

and

$$V = \sqrt{(U^2 + W^2)}. \tag{2b}$$

In the backflow region, the velocity distribution resembles a parabola, V being maximum about midway between the vortex centre and the tube wall.

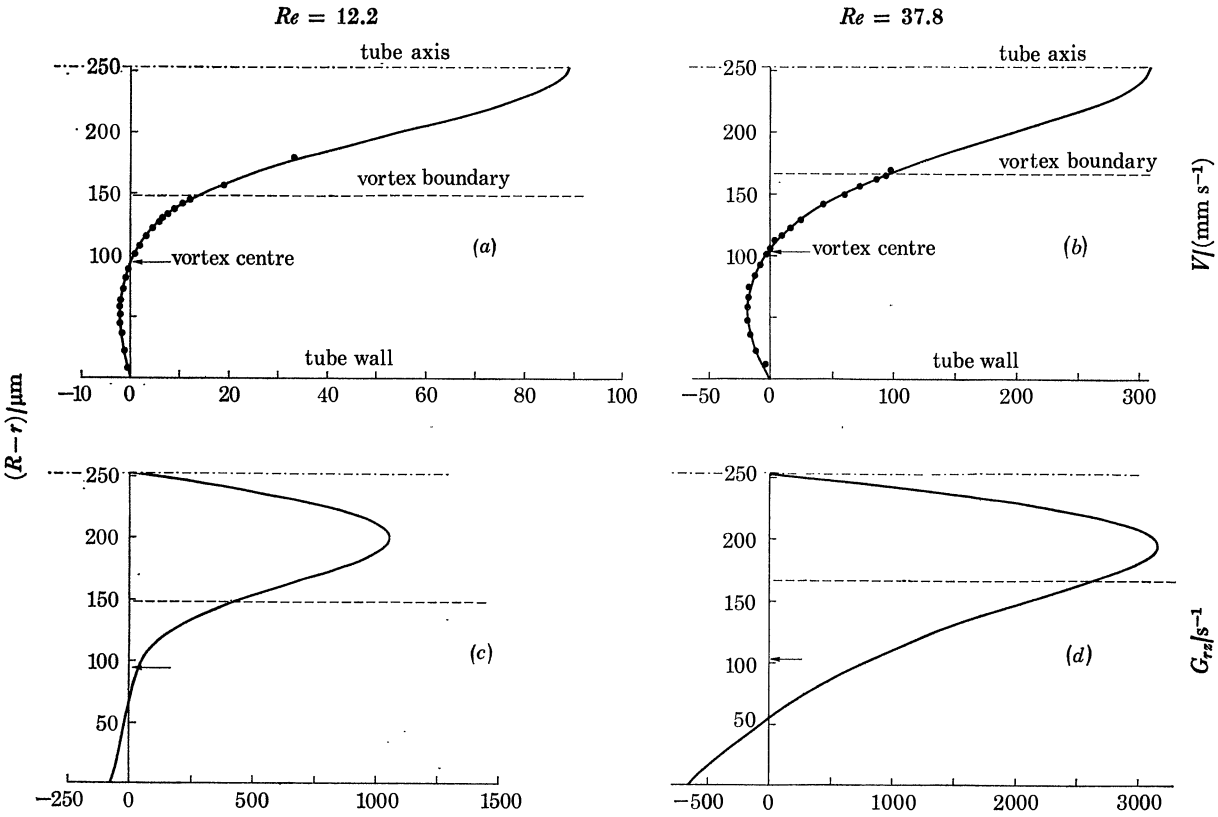

FIGURE 6. Velocity V (a, b) and shearing rate of strain G_{rz} (c, d) in the vortex plotted against distance ($R-r$) from the tube wall along the dashed line PQ shown in figures 2 and 3. The points are the experimental tracer h.b.c. velocities and the curves are calculated from theory (Macagno & Hung 1967).

(iii) *Distribution of shearing rate of strain*

The distribution of the only non-zero component of the shearing rate of strain G_{rz}:

$$G_{rz} = -\left(\frac{\partial W}{\partial z} + \frac{\partial U}{\partial r}\right), \tag{3}$$

was calculated from the theoretical values of the radial and axial velocities at points lying on the line PQ passing through the vortex centre, i.e. where the axial component of the flow predominates (figures 2 and 3). The results for flow at $Re = 12.2$ and 37.8 are plotted in figures 6c and 6d. Unlike the undisturbed flow regions of the tube ($W = 0$), G_{rz} here is not a maximum at the wall. Instead, $G_{rz} < 0$ at the wall; it is zero about midway between the wall and vortex centre and then continuously increases, reaching a maximum on the axial side of the vortex

boundary before finally decreasing to zero at the tube axis. Thus while orbiting, the cells experienced large variations in G_{rz} and hence also in shear stress ($= \eta_0 G_{rz}$), e.g. at $Re = 37.8$ in the orbit in which the backflow velocity is a maximum (the 7th in figure 3), G_{rz} varied from *ca.* 2000 s^{-1} (shear stress *ca.* 2 N m^{-2}) in the forward flowing region to zero in the backflow region.

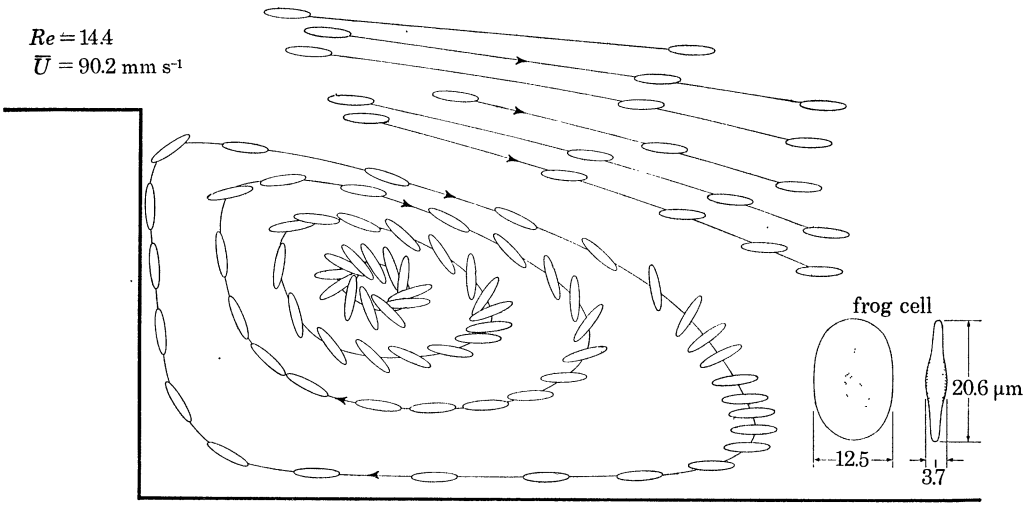

FIGURE 7. Single orbits and orientations of normal frog red cells in the vortex, $Re = 14.4$. *Inset*: diametrical and side view of a nucleated bullfrog red cell with dimensions in μm.

(iv) *Particle rotation and orientation*

The orientations of the h.b.c. as seen in the median plane of the tube were traced from the cine films and are shown drawn on the orbits, for human cells in the upper portions of figures 2 and 3, for the frog cells in figure 7. Although detailed cell shapes could not be discerned at the relatively low magnifications used, it was clear that the cells travelled throughout in an almost edge-on orientation, i.e. with their axes of revolution lying in or close to the median plane of the tube. This facilitated the measurement of the variation in the orientation of the particle major axis with the direction of flow. As indicated schematically in figure 1*c*, we distinguish between an angle of orientation ϕ given by the rZ-projection of the particle axis of revolution with the radial coordinate r of the external flow field, and the orientation angle ϕ' of the rZ-projection of the particle axis of revolution with respect to the normal of the tangent to the contour of a streamline. When the streamlines are parallel to the tube axis, as in the backflow region of the vortex at higher Re (cf. figure 3), $\phi = \phi'$.

With regard to the ϕ-orientation, as expected from the distribution in vorticity (figures 4 and 5) cells in the inner orbits where $\zeta > 0$, rotated in the same direction throughout, $d\phi/dt > 0$, counter clockwise in the upper, and clockwise in the lower half of the median plane of the tube. Cells in the orbits passing through or very close to the point of local maximum backflow velocity where $\zeta = 0$ exhibited no angular rotation in the reverse flow region. In the outermost orbits, $d\phi/dt$ varied continually, and close to the tube wall, where $\zeta < 0$, the direction of angular rotation was reversed.

With respect to the angle ϕ', it was observed that in the inner, almost circular orbits at $Re < 15$ the orientation of the cells with respect to the orbit contour remained constant, $d\phi'/dt = 0$. Most often, as shown in figure 2, the cells were then seen to be aligned in the

direction of flow ($\phi' \approx 0$); occasionally, as shown for the frog cells in figure 7, $\phi' > 0$. The mean period of cell rotation in the innermost orbit, T_c, was determined by measuring the time to execute 5 complete rotations through $\Delta\phi = 2\pi$, and compared with the mean period T_0 for the particle to circulate once around the orbit. As shown in figure 8, for human cells at low Re, $T_c = T_0$; i.e., $d\phi'/dt = 0$, but at $Re > 15$, $T_c < T_0$ as the cell angular velocity $d\phi'/dt$ became appreciable. The quantity $(T_0/T_c - 1)$, which gives the number of cell rotations relative to the streamline during one orbit, is shown plotted inset in figure 8 and increases from the initial zero value with increasing Re. In the case of the frog cells, however, even at the highest Re studied ($= 31$) the measured T_c was still only slightly smaller than T_0.

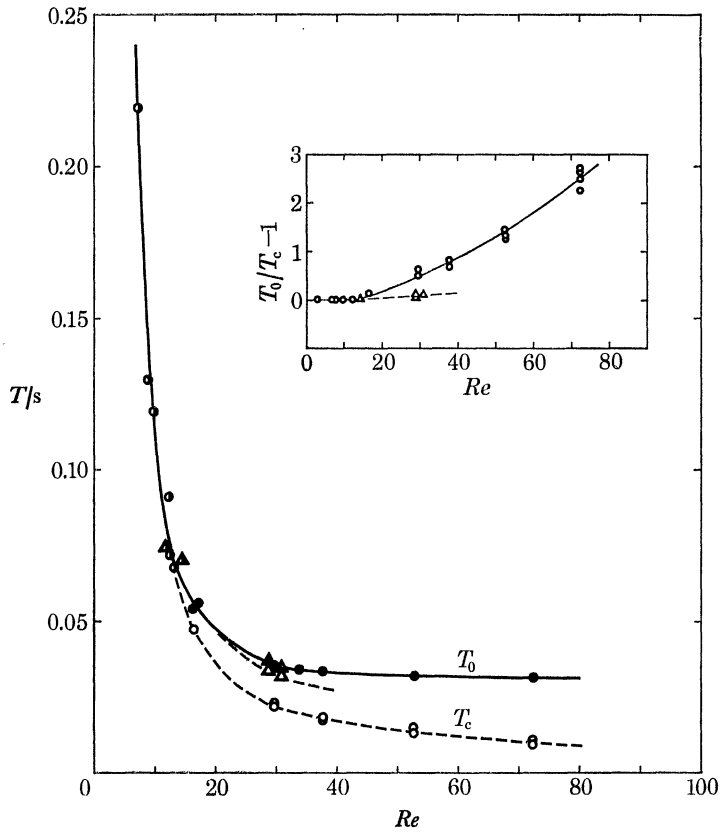

FIGURE 8. Periods of circulation of the orbit, T_0 (● and ▲) and of the cell rotation, T_c (○ and △) for human red cells (circles) and frog red cells (triangles) as a function of Reynolds number. *Inset*: plot of the cell rotation relative to the streamline during one orbit against Re; circles: human cells, triangles: frog cells.

In the outer orbits of the vortex, at positions close to the line PQ (figures 2 and 3), where the streamlines are roughly parallel to the Z-axis, and where flow may approximate that in a simple shear field (the term $\partial U/\partial r$ predominates in equation (3)), the ϕ'-orientations of the h.b.c. changed with time at all Re. The angular velocities $d\phi'/dt$ of the cells in this region of the vortex were measured and compared with those calculated for a rigid spheroid rotating in simple shear flow, assuming Jeffery's theory (1922) to apply:

$$\frac{d\phi'}{dt} = \frac{G}{r_e^2 + 1}(r_e^2 \cos^2 \phi' + \sin^2 \phi'). \qquad (4)$$

Here, r_e is the hydrodynamic, or equivalent ellipsoidal axis ratio (Goldsmith & Mason 1967) which, in a population of h.b.c. has been shown to have a mean value of 0.38 (Goldsmith & Marlow 1972); G is the local shear rate, here assumed to be given by G_{rz} and calculated from equation (3) (Macagno & Hung 1967). The results are given in table 4 and it is evident that except in the orbit closest to the wall, where the measured values are much lower than those calculated, agreement between experiment and theory is surprisingly good considering the fact that the measured $d\phi'/dt$ were obtained over only two or three frames of the film sequence and that $\partial W/\partial z$ is not negligible.

TABLE 4. MEASURED AND CALCULATED ANGULAR VELOCITIES OF h.b.c. IN THE OUTER ORBITS OF THE VORTEX, SYSTEM 1

$Re = 12.2$				$Re = 37.8$			
		$(d\phi'/dt)/(\text{rad s}^{-1})$				$(d\phi'/dt)/(\text{rad s}^{-1})$	
$R-r$ / μm	G_{rz}† / s^{-1}	meas.‡	calc.§	$R-r$ / μm	G_{rz}† / s^{-1}	meas.‡	calc.§
7.0	−70	−20	−45	11	−530	−7.9	−452
22	−50	−2.4	−6.3	34	−270	−65	−61
36	−35	−7.1	−10	57	10	0	5.9
58	−15	−4.7	−3.6	74	240	97	106
72	0	0	0	91	510	255	252
116	110	18	16	115	980	705	609
127	190	35	31	127	1260	510	655
136	275	45	43	142	1660	970	948
142	340	135	99	155	2080	1075	1267
146	395	240	228	164	2370	495	941
157	550	138	130	183	2950	1410	1284
				190	3090	1200	1227
	mean $\frac{\text{meas.}}{\text{calc.}} = 1.10$‖				mean $\frac{\text{meas.}}{\text{calc.}} = 0.92$‖		

† Calculated from theory (Macagno & Hung 1967) using equation (3) at points along the line PQ in figures 2 and 3.
‡ Along the dashed line PQ in figures 2 and 3.
§ From equation (4) assuming $r_e = 0.38$ (Goldsmith & Marlow 1972).
‖ The first value close to the tube wall, not included.

(v) *Migration of blood cells and rigid spheres*

A. *General observations.* As mentioned earlier, tracer single human blood cells in the vortex did not circulate in closed orbits, but over several revolutions could be observed to migrate spirally outward, finally rejoining the mainstream fluid. Eventually, the vortex became depleted of cells, and in order to study this phenomenon it was necessary to give small pulsed disturbances to the flow, thereby refilling the orbits with cells. This outward migration of particles was observed with r.b.c. as well as with h.b.c., with platelets and with latex spheres of diameters $\leqslant 20$ μm. There was no difference between the behaviour of neutrally buoyant particles, and spheres or blood cells lighter or heavier than the suspending fluid (systems 1–3 and 5).

At the same time as the outward radial migration, there occurred a slower but noticeable annular migration of particles into a preferred diametrical plane of the vortex. This resulted in a temporary accumulation of particles in one section of the annulus and there, frequent inter-

actions, especially in the outer orbits led to a large number of particles rejoining the mainstream. The position of the preferred plane in the annulus changed when the flow rate changed. It was thought that such migration was due to a slight asymmetry of the expansion which would result in a secondary flow through the vortex. Hence, attempts were made to construct perfectly axi-symmetric models by machining a metal tube and fitting it concentrically into a 3 mm diameter precision bore glass tube. However, in every case the particles migrated into a preferred plane, although the rate of migration at a given *Re* varied from expansion to expansion. It appears, therefore, that a secondary flow persisted even when the tubes were almost perfectly concentric and cut square.

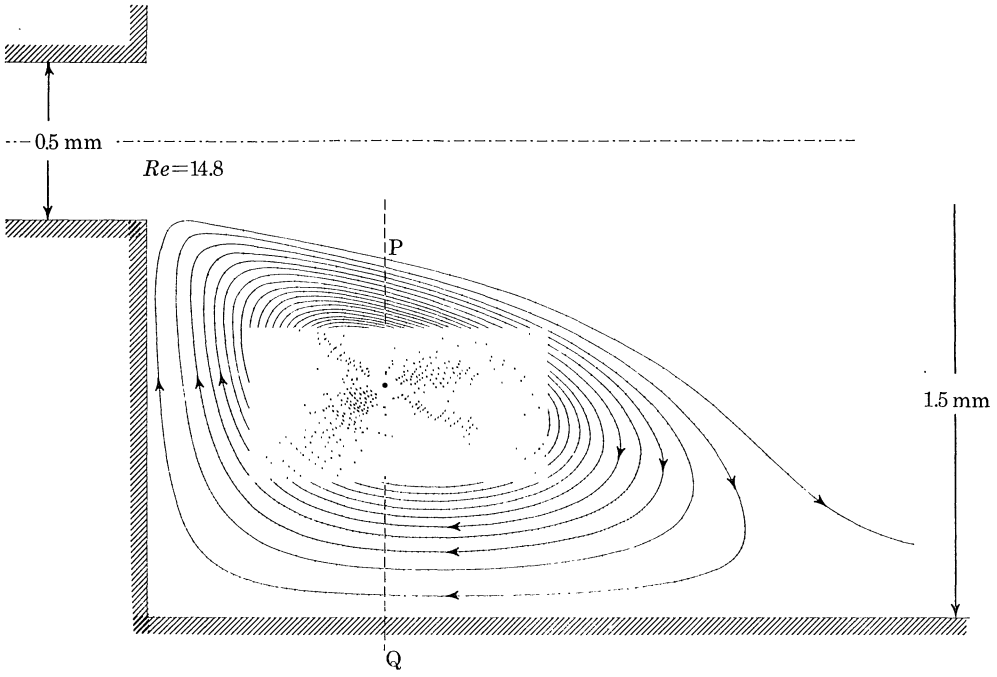

FIGURE 9. Spiral outward migration of a neutrally buoyant, rigid 30 μm diameter carbon sphere in the median plane of the annular vortex at the abrupt expansion of an 0.5 mm into a 3 mm diameter tube; $Re = 14.8$, $\bar{U} = 350$ mm s^{-1}.

In contrast to the behaviour of single small particles, aggregates of red cells larger than about 50 μm in diameter remained within the vortex. At $Re < 10$, the aggregates were situated at the centre but with increasing flow rate they migrated out into preferred orbits where they remained in equilibrium. Upon further increasing *Re*, the aggregates moved back again to the vortex centre, an effect which occurred more rapidly with larger particles. Thus, small aggregates could often be observed in orbit around larger particles located at the centre of the vortex. Annular migration of the aggregates was also observed.

Finally, it was noted that at the highest Re (> 70) asymmetric, irregularly shaped, large aggregates precessed in an annulus at right angles to the direction of flow, while themselves rotating with very high angular velocity. This observation, never made with spherical particles or symmetrical aggregates, is illustrated schematically in figure 12*e*.

To obtain further insight into the above described phenomena, experiments on the migration paths and residence times of particles within the vortex were carried out.

B. *Migration path and velocity*. This was studied in detail using model carbon spheres in system 6, and an expansion of a 0.5 mm into a 3.0 mm diameter tube. The migration, in a spiral of

slowly increasing diameter, of a 30 μm carbon sphere is shown in figure 9. The particle, initially close to the vortex centre, at first migrated out quite slowly, and then with increasing velocity as the diameters of succeeding orbits increased appreciably. The rate of migration is illustrated in figure 10 in which the radial distance $(r_0 - r)$ of the particle from the vortex centre (along the dashed line PQ shown in figure 9) is plotted against time. The 'migration velocity', dr/dt, at $Re = 14.8$ ranged from ± 20 μm s^{-1} near the centre to a maximum of 75 μm s^{-1} and 150 μm s^{-1} on the axial and wall sides of the vortex.

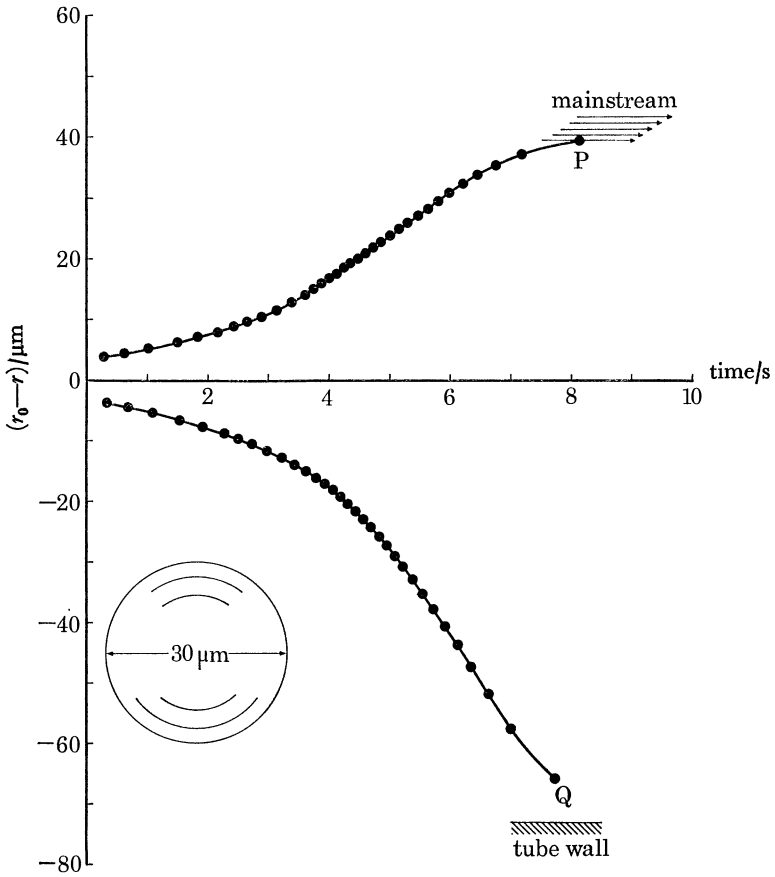

FIGURE 10. The outward migration of the carbon sphere shown in figure 9 plotted as the distance of the particle from the vortex centre along the line PQ (figure 9) against time.

C. *Residence times*. Neutrally buoyant, monodisperse suspensions of polystyrene latex spheres (system 7) having diameters of 2.6, 9.8, 20, 32 and 50 μm (± 10 %, s.d.) were used to measure the effects of particle size and flow rate on the residence times in the annular vortex in the 151 μm to 504 μm diameter sudden expansion. The measurements were made by giving a small sharp disturbance to the flow, thereby filling the vortex with particles, and then observing the migration of the spheres out of the vortex. A residence time τ was defined as the time interval between the onset of the disturbance and the last particle leaving the vortex. It should be noted, however, that most of the spheres left the vortex at times $t \ll \tau$. Mean values of τ were obtained from 20 or more measurements. As shown in figure 11 for the 2.6 μm spheres, the standard deviation from the mean τ was high. This was no doubt due to differences in the times to migrate out of the vortex for particles initially located in outer orbits and those starting from the centre when the disturbance was first given.

The results showed that in a given tube and for suspensions of the smaller spheres, there was an initial decrease in the mean residence time with increasing *Re* (< 10), presumably because of the rapidly decreasing orbit circulation times T_0 (cf. figure 8). A minimum in $\bar{\tau}$ was reached at an *Re* which depended on the particle diameter, being smallest for the 20 μm spheres (figure 11). A further increase in flow rate then led to a very rapid rise in $\bar{\tau}$ until at a critical *Re* (also particle-size dependent) a single sphere remained indefinitely within the vortex circulating in an outer orbit. All other particles had been eliminated, apparently through interactions between spheres in the peripheral orbits of the vortex. Thus, while particles migrated out of the vortex, two-body collisions were observed and these resulted either in a change of the trajectories of the participating spheres which then rejoined the mainstream, or in the formation of non-separating doublets (Goldsmith & Mason 1964) which migrated to the vortex centre where they remained. In the case of the 20 μm spheres, the last remaining particle circulated in an equilibrium orbit close to the boundary of the vortex (figure 12*a*). With the 2.6 and 9.8 μm spheres, this equilibrium orbit appeared to be close to the streamline passing through the point of maximum backflow velocity (figure 12*b*). Sometimes, the last of the smaller spheres was located at the vortex centre, but this was an unstable equilibrium position.

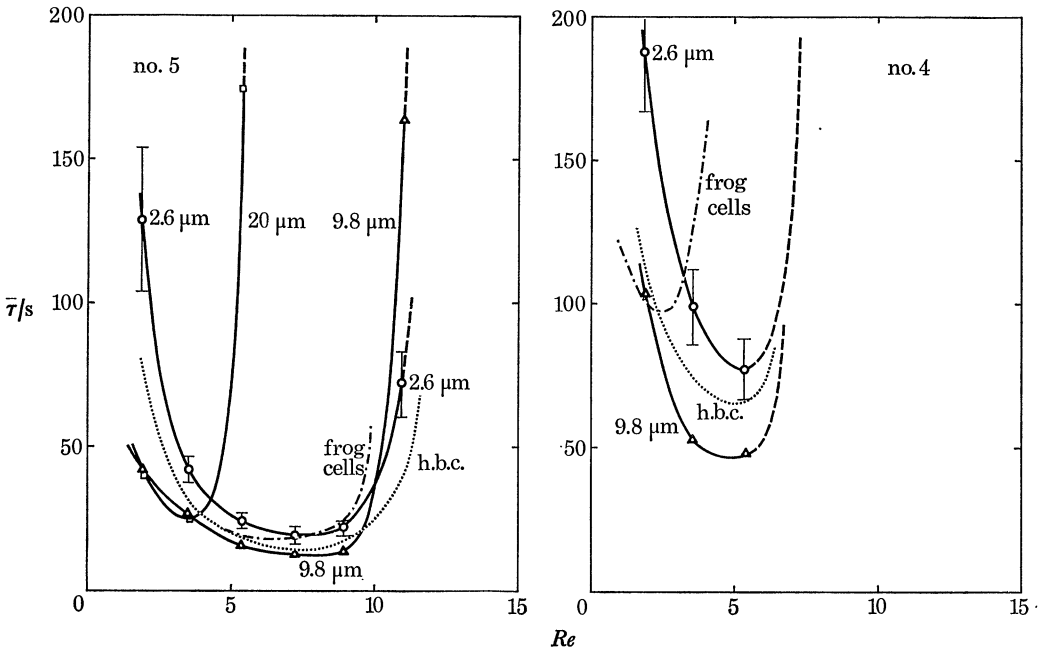

FIGURE 11. Mean residence times, $\bar{\tau}$, of latex spheres, h.b.c. and frog red cells in the annular vortex at the abrupt expansion of a 151 μm tube into a 504 μm tube, as a function of Reynolds number. *Left*: expansion no. 5 in which the *annular* migration as well as the outward *radial* migration was greater than in expansion no. 4, shown on the right. The bars on the curve for the 2.6 μm sphere represent ± 1 standard deviation.

When the flow rate was increased above the critical *Re*, more particles stayed in the vortex and circulated in equilibrium orbits on various diametrical planes in the annulus. In the case of the 20 μm spheres the orbits shifted inward to the streamline corresponding to maximum backflow velocity, and at $Re \approx 70$ two stable equilibrium positions appeared (figure 12*c*): one in which the particles circulated in an equilibrium orbit as before, and the other at the vortex centre. These positions were interchangeable as was shown by slightly disturbing the

flow when the spheres migrated from the orbit to the centre and vice versa. At still higher *Re*, the vortex centre became the more stable position and many of the particles migrated there. At $Re > 110$ the vortex was filled with very many spheres and these were continually displaced from their orbits and to and from the centre as particle interactions and collisions became very important.

In the case of the 2.6 μm and 9.8 μm spheres the results were similar except that here the vortex centre was not a stable position at the higher *Re*. Instead, the number of particles remaining in the vortex in equilibrium orbits increased with increasing *Re* until at $Re > 65$ the vortex was filled with spheres, and now aggregates were observed to form and to migrate to the centre.

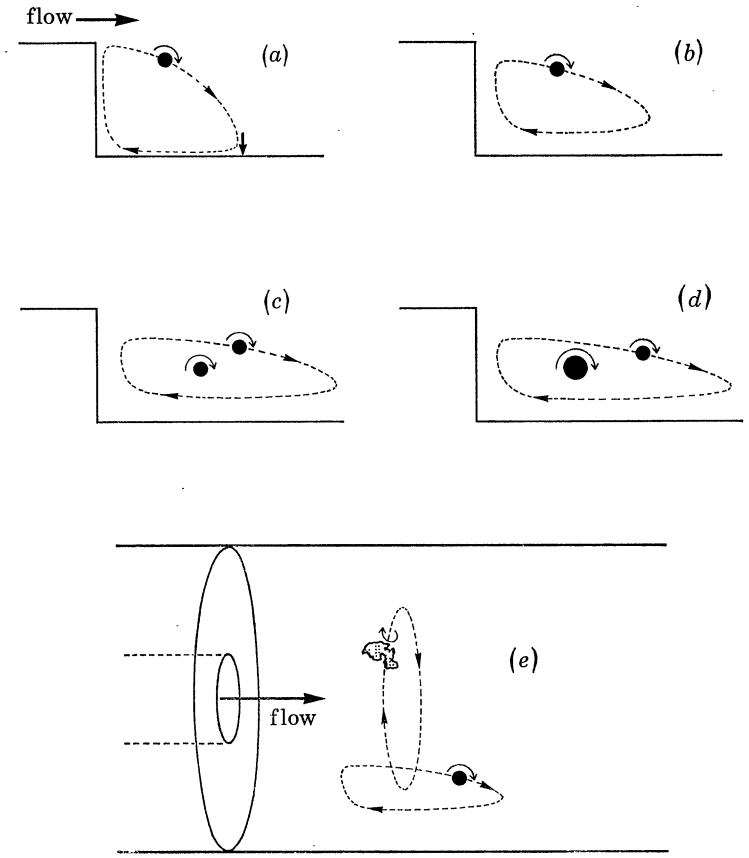

FIGURE 12. Schematic representation of equilibrium orbits of latex spheres and aggregates within the annular vortex as the Reynolds number is increased from (*a*) to (*e*). (*a*) equilibrium orbits at the boundary and (*b*) at the position corresponding to maximum backflow velocity. (*c*) Two stable orbits seen with spheres having diameters $\geqslant 20$ μm. (*d*) Orbiting of smaller sphere around a larger particle at the centre. (*e*) Precessing annular motion of an asymmetric irregular-shaped aggregate of h.b.c.

By contrast, the larger 32 μm and 50 μm spheres remained in the vortex at all *Re* studied, from < 1 to 120. For $1 < Re < 50$, only one or two particles remained circulating first in the boundary and then in the smaller diameter equilibrium orbits. At higher *Re*, the two equilibrium positions seen with the 20 μm spheres were observed and finally at $Re > 100$ the vortex was filled with particles.

Experiments were also carried out with a mixture of the 9.8, 20 and 32 μm sphere suspensions and here at low *Re* (*ca.* 7) single 32 μm particles remained in the vortex in an equilibrium orbit.

PHILOSOPHICAL TRANSACTIONS OF THE ROYAL SOCIETY B BIOLOGICAL SCIENCES

At $Re \approx 90$, as shown in figure 12*d*, 9.8 and 20 μm spheres circulated in orbits about a 32 μm sphere situated at the centre. Here it was also observed that appreciable inward migration of the larger latex spheres had occurred in the 151 μm tube upstream of the expansion. Only the 2.6 μm spheres entered the expansion on streamlines close to the boundary of the vortex, but they were never seen entering the region of separated flow.

As illustrated in figure 11, the values of the mean residence times in a given suspension varied from tube to tube; $\bar{\tau}$ at a given Re was significantly greater in an expansion in which the rate of annular migration was lower. In the example given in figure 11, Re corresponding to the minimum $\bar{\tau}$ decreased from *ca.* 8 to *ca.* 5 for the 9.8 μm spheres, and in the apparently more axisymmetric expansion (no. 4), single 20 μm spheres remained within the vortex even at the lowest Re studied.

Measurements of $\bar{\tau}$ were also made with h.b.c. and frog red cells, and with human platelets. The results for the red cells were similar to those obtained with the latex spheres, the behaviour of the h.b.c. being intermediate between those of the 2.6 and 9.8 μm spheres (figure 11), and as with the latex spheres at low Re, there was an unstable equilibrium position at the vortex centre. The larger, ellipsoidal frog cells (cf. figure 7) took equilibrium orbits inside the streamline corresponding to maximum backflow velocity, as well as at the vortex centre, and the values of $\bar{\tau}$ at a given Re were intermediate between those of the 9.8 μm spheres and the h.b.c. In the case of the platelets, especially those suspended in heparinized plasma, the continuous formation and accumulation of small aggregates within the vortex made it difficult to measure meaningful residence times. Nevertheless, it was clear that single platelets migrated out of the vortex at the lower Re, and when the experiment was repeated in citrated plasma at pH = 6.5, aggregation then being suppressed, all the platelets left the annular vortex.

(*b*) *Pulsatile flow*

The axial velocity $U(r, t)$ at a radial distance r and at time t of a fluid undergoing pulsatile flow (steady flow superimposed on oscillatory flow) in a circular tube of radius R is given by (Womersley 1955; Shizgal, Goldsmith & Mason 1965)

$$U(r, t) = \frac{BM_0'}{\rho_0 \omega} \sin\left[\omega t + \epsilon_0(\alpha, r/R)\right] + \frac{B_0}{4\eta_0}(R^2 - r^2). \tag{5}$$

Here α is the dimensionless parameter defined by

$$\alpha = R\left(\frac{\omega \rho_0}{\eta_0}\right)^{\frac{1}{2}},$$

and

$$B_0 = \frac{8\eta_0 Q_0}{\pi R^4},$$

where Q_0 is the steady volume flow rate; ρ_0 and η_0 are the respective density and viscosity of the fluid and $\omega = 2\pi f$, the angular velocity of the oscillatory flow at a frequency of f cycle s^{-1}, B is the amplitude of the oscillatory pressure gradient which may be calculated from the volume displacement per half cycle, ΔV, using the relation

$$B = \frac{\Delta V \eta_0}{2\pi R^4} \frac{\alpha^2 \omega}{M_{10}'}. \tag{6}$$

M_{10}' is a function of α and has been tabulated (Womersley 1955); M_0' and the phase angle ϵ_0 are functions of α and r/R, and can be calculated from tables of Bessel functions.

PHILOSOPHICAL TRANSACTIONS OF THE ROYAL SOCIETY B BIOLOGICAL SCIENCES

The behaviour of blood cells in systems 1, 3 and 4 were studied in pulsatile flow under conditions in which the relative magnitudes of the amplitude of the oscillatory volume flow rate $Q^* = \frac{1}{2}\Delta V\omega$ and the steady flow rate Q_0 were adjusted so that there was no backflow into 151 μm tube except at the lowest Q_0. This avoided any complications arising from an annular vortex formed in the convergent flow at the end of the cycle (Christiansen, Kelsey & Carter 1972). Within this restriction, the effects of varying ΔV and f on the flow patterns and on particle

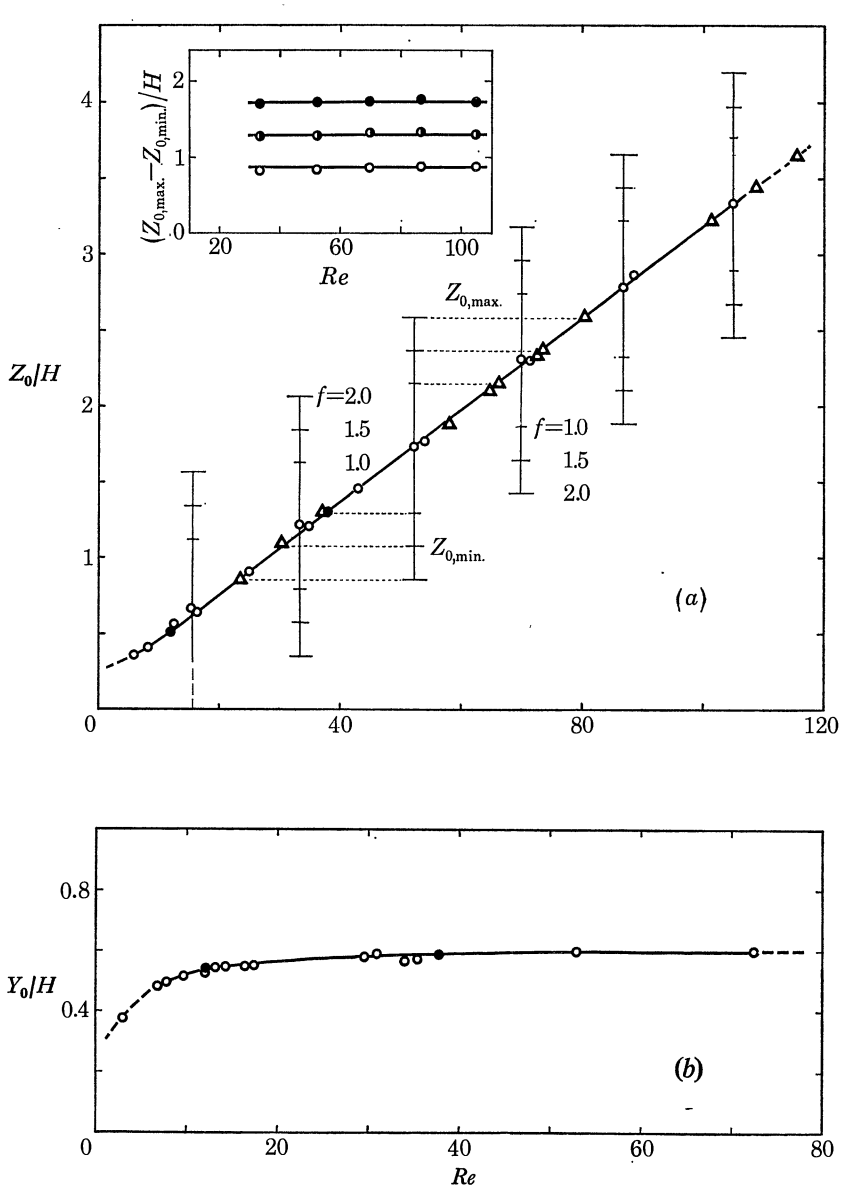

FIGURE 13. (*a*) Axial and (*b*) radial positions of the vortex centre in steady flow as a function of Reynolds number; H = 176 μm. The open circles are experimental points, the closed circles are values calculated at Re = 12.2 and 37.8 respectively (Macagno & Hung 1967). The horizontal bars in part (*a*) are the maximum and minimum Z_0 in pulsatile flow at frequencies of 1.0, 1.5 and 2.0 cycle s^{-1} respectively, and for ΔV = 0.5 μl. The triangles are the measured Z_0 plotted against Re calculated by using the upstream mean maximum and minimum linear velocities in pulsatile flow. *Inset*: plot of the amplitude in Z_0 against Re: ○, f = 1.0; ◑, f = 1.5; ●, f = 2.0 cycle s^{-1}.

migration were studied. Frequencies from 0.5 to 3 cycle s^{-1} were used; these corresponded to α (R = 250 μm) from 0.5 to 1.1; i.e. inertial effects upstream and downstream of the vortex were not pronounced, ϵ_0 being close to 0 at all r/R.

(i) *Oscillation and size of the vortex*

The vortex changed in size and intensity periodically, with the axial location of the centre, Z_0, and the reattachment point, L, oscillating between maximum and minimum positions about

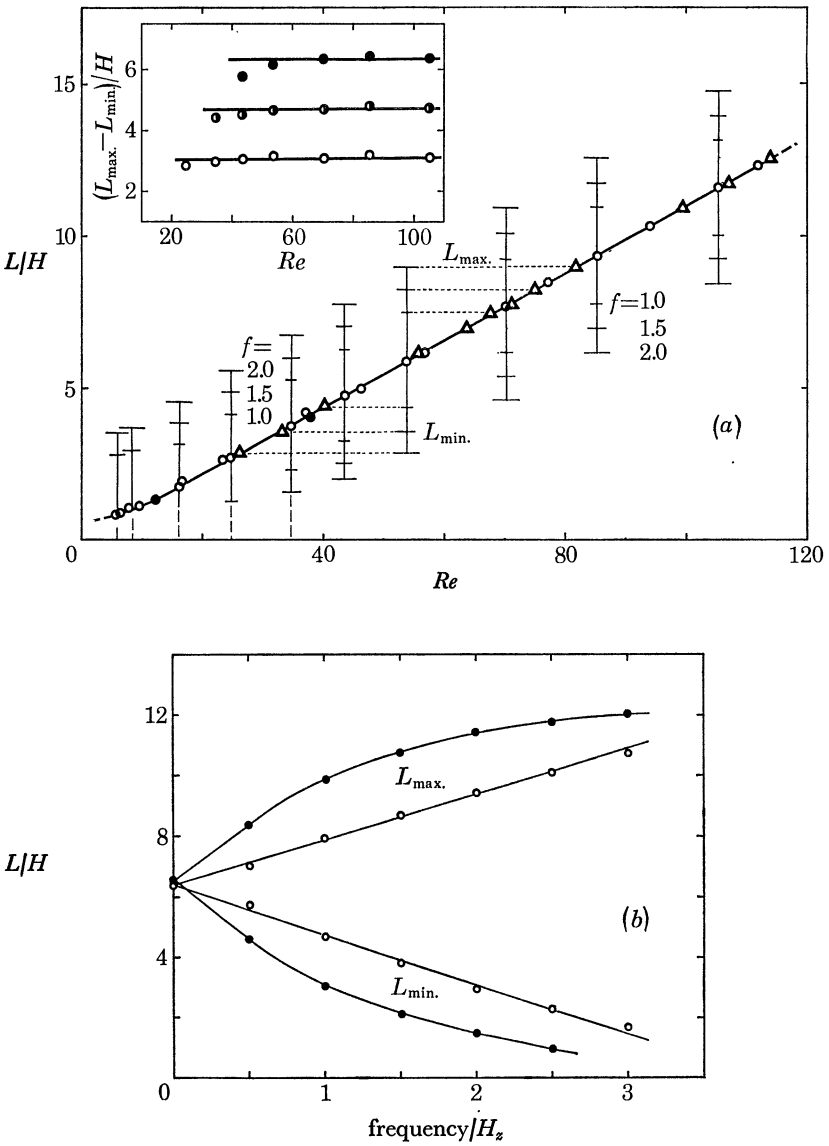

FIGURE 14. (*a*) Dimensionless vortex length, L/H, as a function of Reynolds number in steady flow (○) and maximum and minimum L in pulsatile flow (horizontal bars) at f = 1.0, 1.5 and 2.0 cycle s^{-1} respectively; ΔV = 0.5 μl, H = 176 μm. As in figure 13, the closed circles are calculated values at Re = 12.2 and 37.8 respectively and the triangles are the measured L plotted against a pulsatile flow Reynolds number using the upstream mean linear velocities. *Inset*: plot of the amplitude in L against Re: ○, f = 1.0; ◑, f = 1.5; ●, f = 2.0 cycle s^{-1}. (*b*) The vortex length, L, as a function of frequency at ΔV = 0.5 (○) and 1.0 μl (●); Re = 57.5.

a mean which corresponded to the vortex in the absence of the oscillatory flow component. The vortex reached maximum and minimum size at values of $\omega t = \frac{1}{2}\pi$ and $\frac{3}{2}\pi$ respectively, corresponding to the maximum and minimum in fluid velocity (equation (5)). The values of Z_0 and L during a cycle were determined from the motion of the individual human h.b.c. recorded on cine film, and within the experimental error of $\omega t = \pm 5°$, there was no measurable phase lag of the centre or the reattachment point with fluid velocity, even at $f = 3$ cycle s^{-1}.

The results of the variation in Z_0 and L with Re in steady and pulsatile flow are shown plotted in figures 13*a* and 14*a* in dimensionless form (divided by the step height H). As predicted by theory (Macagno & Hung 1967), Z_0 and L increased linearly with increasing Re in steady flow. The theoretical values for $Re = 12.2$ and 37.8 lie on the best fit line drawn through the experimental points. Extrapolation to zero Re indicated, that both Z_0 and L had non-zero values in the creeping flow regime. In pulsatile flow, the maximum and minimum Z_0 and L, indicated by the bars on the vertical lines in the figures, lay symmetrically about the values obtained in steady flow. For $\Delta V < 1.0$ µl, the amplitudes in Z_0 or L were virtually independent of Q_0 (see inset, figures 13*a* and 14*a*), being greater for the oscillation of the reattachment point than for the vortex centre. Moreover, as shown in figure 14*b*, the amplitudes at a given Q_0 increased linearly with increasing frequency up to $f = 2$ cycle s^{-1}, and when a Reynolds number for pulsatile flow at maximum and minimum fluid velocity was calculated using the mean linear upstream velocity $\bar{U} = (Q_0 \pm Q^*)/\pi R^2$, the values of Z_0 and L at $\omega t = \frac{1}{2}\pi$ and $\frac{3}{2}\pi$ could be fitted into the line drawn for steady flow (triangles in figures 13*a* and 14*a*). At $\Delta V \geqslant 1$ µl, however, the amplitude in Z_0 and L no longer increased linearly with increasing frequency at a given Q_0 (figure 14*b*).

Finally, figure 13*b* shows the variation in the radial location of the vortex centre, Y_0, with increasing Re: below $Re = 15$, Y_0 increased rapidly with increasing Re, but then asymptoted to a steady value at $Y_0 \approx 0.6H$. As expected from this result, the amplitude in Y_0 during pulsatile flow was very small and is not shown in the figure.

(ii) *Particle migration*

As in steady flow, so in pulsatile flow h.b.c. and latex spheres < 30 µm diameter migrated out of the vortex, whereas aggregates of cells and spheres > 30 µm diameter continued to orbit within the vortex at all frequencies at a given steady flow rate. At low amplitudes ($\Delta V < 1$ µl) the rate at which the vortex emptied of h.b.c. in dilute suspensions increased at first with increasing f, but when $f > 2$ cycle s^{-1}, the vortex contained particles during the whole of the cycle. As f increased further, their number increased markedly. The critical frequency at which cells remained within the vortex decreased with increasing amplitude of the oscillatory flow.

The orbits of single h.b.c. and aggregates within the vortex in pulsatile flow are shown in figure 15. A cell, initially situated at a point A (outside the streamlines of the vortex in steady flow), just after the beginning of the growth of the vortex ($\omega t = -71°$) was caught up in advancing vortex and followed a series of expanding spiral orbits reaching the furthest point B just after the end of the forward movement ($\omega t = 90°$). During the recession of the vortex, the cell executed a series of shrinking spiral orbits, the last of which took the particle to a position outside the boundary of the retreating vortex as it changed direction ($\omega t = 270°$), and the cell rejoined the mainstream along the streamline CDE. Cells were observed to migrate radially outward during the advance of the orbit down the tube and often left the region of

PHILOSOPHICAL TRANSACTIONS OF THE ROYAL SOCIETY B BIOLOGICAL SCIENCES

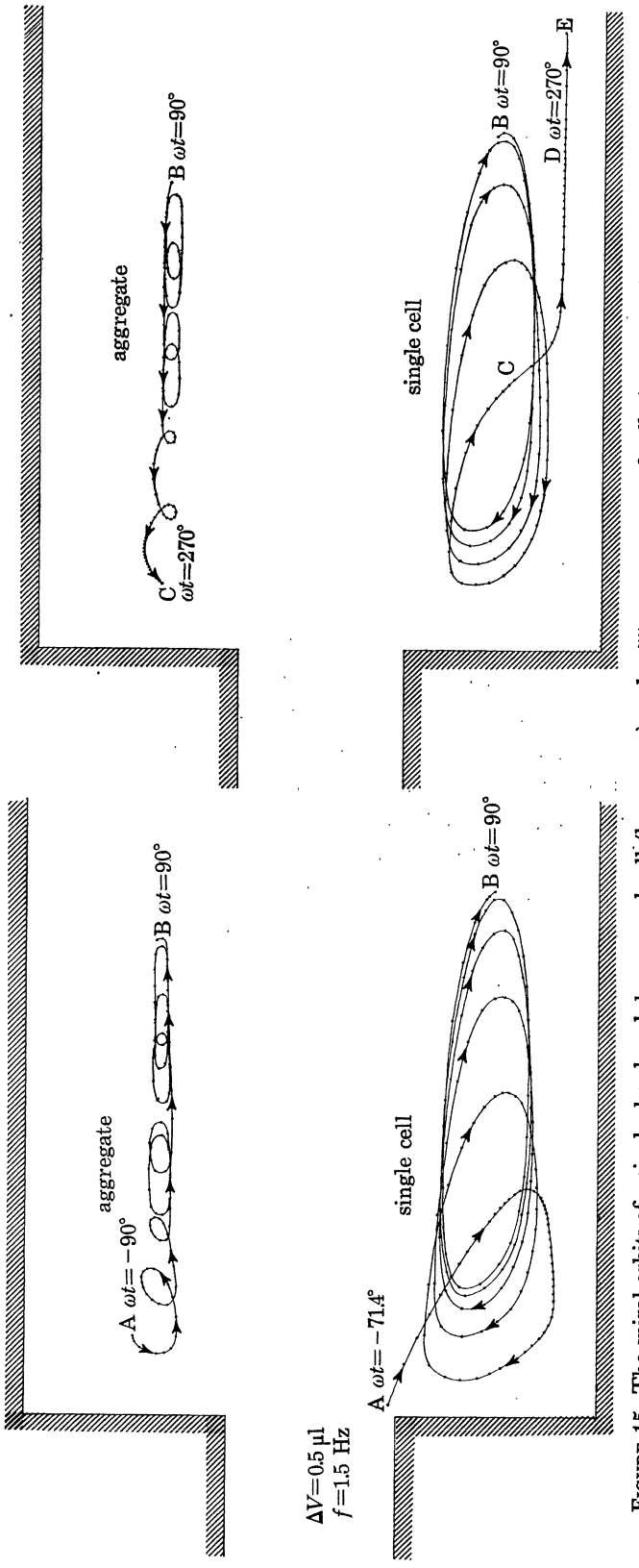

FIGURE 15. The spiral orbits of a single, hardened, human red cell (lower part) and a 55 µm aggregate of cells (upper part) in pulsatile flow during the advance (left) and recession (right) of the vortex during one cycle; $\Delta V = 0.5$ µl, $f = 1.5$ cycle s^{-1}, Re (steady flow component) = 38.4 (upper) and 23.2 (lower). The positions of the particle at various portions of the cycle are indicated.

separated flow; others reached an outer orbit only at $\omega t \approx 90°$. Such particles, travelling slowly backward near the tube wall, were sometimes left behind as the reattachment point gained increasing speed and passed them by. Conversely, as the vortex grew in size some cells in the mainstream were caught up into the vortex. At $f < 2$ cycle s^{-1}, it was evident that the cell concentration within the vortex was smaller in the advancing than in the receding period and was at all times lower than in the mainstream of the flowing suspension. With increasing Q_0 the rate at which the particles migrated out during the advance of the vortex increased.

In contrast, the path of an aggregate of h.b.c. of *ca.* 55 μm diameter, which remained within the oscillating vortex, is illustrated in the upper half of figure 15. The particle executed a series of spiral orbits close to the centre of the advancing vortex from a position A at $\omega t \approx -90°$ to B at $\omega t \approx 90°$. When the vortex retreated again, the aggregate remained near the centre, following a series of spiral orbits which took it back to a position C close to its starting point.

(*c*) *Concentrated suspensions of red cells*

A few qualitative studies were carried out with suspensions of red cells in platelet-poor plasma at haematocrits from 15 to 30 %, and with whole blood at 45 % haematocrit.

(i) *Steady flow*

As in the dilute suspensions at low Re (< 10), so at the higher concentrations red cells were observed to migrate out of the vortex, sometimes leaving a completely cell-free annular region as illustrated at 20 % haematocrit in the photomicrographs of figure 16*a*, plate 1, at other times leaving a few aggregates (rouleaux) behind circulating in equilibrium orbits. The initial decrease in red cell concentration occurred first near the reattachment point, and after 15–20 s at $Re = 1.5$, 10–15 s at $Re = 4.5$, and 20–25 s at $Re = 9$, the vortex was completely depleted of single cells. The times for the vortex to empty of r.b.c. at a given Re increased with increasing haematocrit. Owing to the existence of a cell-free vortex, and the fact that no particles entered the expansion on streamlines close to its boundary, a cell-free plasma layer developed at the tube wall downstream of the reattachment point. The thickness of this layer at $Re = 0.5$ varied from *ca.* 7 μm at 45 % haematocrit to *ca.* 10 μm at 20 % haematocrit.

At $Re > 10$, red cells remained in the vortex region and it appeared that some cells were entering from the mainstream while others migrated out. An equilibrium concentration was established which increased with increasing Re.

It was also noted that a tiny secondary annular vortex existed at the corner of the expansion enclosed by the larger primary annular vortex and the wall. Normally, this region was devoid of cells, but by giving a sharp disturbance to the flow, cells could be trapped in this area and were observed to circulate in small orbits in a direction opposite to that of cells in the primary vortex. The length of the triangular shaped, secondary vortex was about 30 μm at $Re = 25$, at which flow rate the length L of the major vortex was 560 μm.

In the case of heparinized whole blood, the interesting observation was made that platelet aggregates containing some red cells formed and grew to occupy a large section of the annular vortex. These large thrombi were not seen in citrated whole blood.

(ii) *Pulsatile flow*

The periodic changes in vortex size and intensity were here accompanied by variations in red cell concentration: the haematocrit was lower in the advancing than in the receding period,

PHILOSOPHICAL TRANSACTIONS OF THE ROYAL SOCIETY B BIOLOGICAL SCIENCES

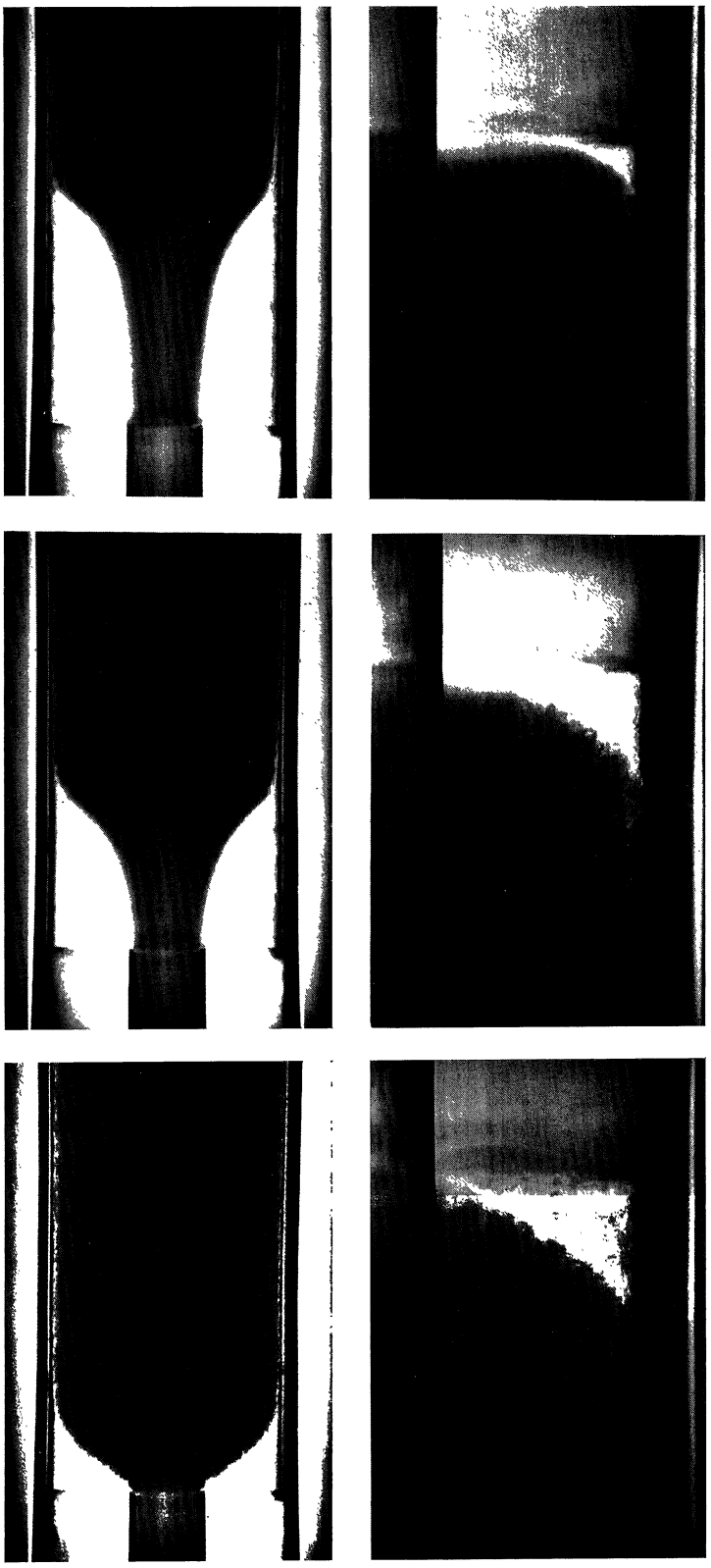

FIGURE 16. Photomicrographs of a 20 % red cell suspension in steady flow through the 151–504 μm tube expansion (*a*), and in convergent flow through the same tubes (*b*). The Reynolds number increases from left to right, the values being: (*a*) 1.5, 9.0, 13.5; (*b*) 0.5, 1.5, 13.5.

(*Facing p.* 438)

PHILOSOPHICAL TRANSACTIONS OF THE ROYAL SOCIETY B BIOLOGICAL SCIENCES

and at all times lower than that in the mainstream. At a given amplitude of the oscillatory flow, the concentration of red cells in the vortex increased with increasing frequency and reservoir haematocrit.

(*d*) *Convergent flow*

Some observations of the flow patterns in concentrated red cell suspensions entering the sudden constriction of a 504 to a 151 μm diameter tube were also made. As expected in this convergent flow (Christiansen *et al.* 1972), an annular vortex was formed at the corner of the constriction whose size decreased with increasing *Re*, as illustrated in figure 16*b* for blood at 20% haematocrit. As in the expansion flow, outward migration of red cells was observed. In whole blood at 45% haematocrit, the vortex was filled with cells at low *Re* (*ca.* 1–1.5) except for a small region around the separation point. With increasing flow rate, particle migration increased and at $Re = 20$, a small cell-free vortex developed. In a 20% suspension, the cell migration was much more pronounced (figure 16*b*), and already at $Re = 1.5$ a cell-free annular vortex developed within two minutes; this time decreased to *ca.* 40 s at $Re = 4.5$.

In addition, a very small secondary annular vortex, similar to that observed in expansion flow, was observed at the corner of the constriction. This vortex, usually free of red cells, was about 20 μm long at $Re = 1.5$ when the length L of the primary vortex was 290 μm. With increasing *Re* the secondary vortex disappeared.

4. Discussion

Results have been presented on the size and shape of an annular vortex seen in the common median plane of a sudden concentric expansion when suspensions of red cells, platelets and rigid spheres are subjected to steady and pulsatile flow. In steady flow, the location of the vortex centre, the reattachment point and the velocity distributions were in good agreement with theory. In pulsatile flow, the vortex appeared to oscillate in phase with the upstream fluid velocity $U(r, t)$, symmetrically about a location corresponding to its position in the absence of the oscillatory flow component. The most interesting and novel observations, however, and those which prompted this investigation, were concerned with the migration of red cells, platelets and rigid spheres across the fluid streamlines of the annular vortex. Such radial migration, dependent in magnitude and direction on Reynolds number and particle size, may have interesting implications for the dynamics of blood flow in arteries. Before dealing with this question and the possible mechanism underlying particle migration, the observations on cell orientations in the vortex are first discussed.

(*a*) *Cell rotation and orientation*

Close to the vortex centre at low *Re*, human red cells rotated through $\Delta\phi = 2\pi$ while maintaining a constant orientation ϕ' with respect to the streamline (figure 2). The measured period of rotation of the cell, T_c, and the time T_0 to circulate once around the orbit were identical. Moreover, since T_0 was almost constant for the first three orbits plotted (up to a radial distance of about 30 μm from the centre) this suggested the existence of a region of rigid-body rotation in which the fluid elements moved with constant angular velocity $\Omega = \frac{1}{2}\zeta'_\theta$. In such an idealized flow, the orbit time of both fluid elements and small tracer particles would be identical, given by $T_0 = 2\pi/\Omega$ and ϕ' would be constant. With the calculated $\zeta'_\theta = 166$ rad s^{-1} at the centre of the vortex at $Re = 12.2$, this yields $T_0 = 0.076$ s, compared to the measured value of 0.090 s

PHILOSOPHICAL TRANSACTIONS OF THE ROYAL SOCIETY B BIOLOGICAL SCIENCES

for an h.b.c. in the smallest orbit studied (table 3). In fact, calculations show that the vorticity is not constant in this orbit, but varies from 135 to 185 rad s^{-1}. Flow at the lower *Re* thus only approximates that in a region of rigid-body rotation.

The preferred orientation of the h.b.c. and the frog cells in the direction of flow, often observed in the orbits of the vortex, may be explained by analogy with the case of a simple shear flow. Here, theory (Jeffery 1922) predicts that the angular velocity of an oblate spheroid (equation (4)) is r_e^{-2} times smaller at $\phi' = 0$ when the particle is aligned with the flow, than at $\phi' = \frac{1}{2}\pi$ when the spheroid lies across the direction of flow. The angular velocities would thus be 6.9 times smaller for the h.b.c. and 83 times smaller for the frog cells ($r_e = 0.11$; Goldsmith, Cox & Doubilet 1976). In a shear flow, these particles would spend 27 % and 64 % respectively, of their time aligned between $\pm 10°$ of the direction of flow. It is not surprising, therefore, that as shown in figure 8 (inset) for the frog cells, $T_c \approx T_0$ even at $Re = 31$.

(*b*) *Radial migration of particles*

It appears probable that the outward radial migration of blood cells and spheres within the vortex is in part related to a secondary flow caused by imperfections in the geometry of the expansion. This flow leads to a drift of particles into preferred planes in the annulus, and the more rapid this drift the more rapid the migration of particles out of the vortex. Such an hypothesis, however, cannot explain the existence of a critical Reynolds number above which particles remained in stable orbits within the vortex. Rather, it is necessary to postulate an opposing inward migration which is dependent on both particle size and Reynolds number. Since the observed effects are certainly not due to centrifugal forces (which even in the non-neutrally buoyant systems were negligibly small) one must look for an explanation in terms of particle interactions with the tube wall and the effects of fluid inertia.

Lateral particle migration due to inertia has been described in dilute suspensions of rigid spheres and cylinders (Brenner 1966; Goldsmith & Mason 1967) and of human red cells (Goldsmith & Mason 1971) undergoing Poiseuille flow. In neutrally buoyant systems, the particles are observed to migrate inward from the wall and outward from the axis to an eccentric radial equilibrium position at $r \approx 0.6R$. As mentioned above, inward migration of the latex spheres occurred in the 151 μm tube and no particles entered the expansion on streamlines close enough to the boundary of the vortex for a secondary flow to have taken them into and through the region of flow separation.

Theories attempting to explain the two-way radial migration in this, so called 'tubular pinch effect' (Segré & Silberberg 1962), must take into account the presence of the tube walls. This was first done by Cox & Brenner (1968) who gave expressions for the rate of migration of rigid spheres in Poiseuille flow by making a double expansion of the flow field in terms of the particle Reynolds number and particle to tube size ratio. The results were not evaluated explicitly but were left in the form of volume integrals involving the Green's function for creeping flow in the tube. The theory has since been extended by calculating analytically the migration velocity of a rigid sphere in a flow near a single vertical plane wall (Cox & Hsu 1976) and for flow between two parallel plane walls (Vasseur 1973). It is the former case, which can be qualitatively applied to particle behaviour in that section of the vortex in which flow is virtually parallel to the tube wall (regions I and II in figure 17) and in which the velocity distribution has the form $U(y) = ay - cy^2$, $y = (R - r)$ being the distance of the particle centre from the wall.

The theory calculates migration velocities in terms of the particle Reynolds number

$Re_p = bU_M\rho_0/\eta_0$ and the length scale ratio b/y, U_M being the maximum fluid velocity at a distance $y = y_M$. Providing $Re_p \ll b/y \ll 1$, the theory predicts that neutrally buoyant, freely rotating spheres close to the wall migrate inward, and those close to the line of maximum velocity migrate outward to a position of stable equilibrium $y^* = \frac{22}{73}y_M$ (*ca.* $0.3y_M$). At $y = y_M$ there is a position of unstable equilibrium, and at $y > y_M$ migration is in a direction away from the wall. The migration velocity is given by (Cox & Hsu 1976):

$$\frac{dr}{dt} = \frac{5}{288} Re_p U_M \left(\frac{b}{y}\right)^2 \beta^2(1-\beta)(22-73\beta), \tag{7}$$

where $\beta = y/y_M$.

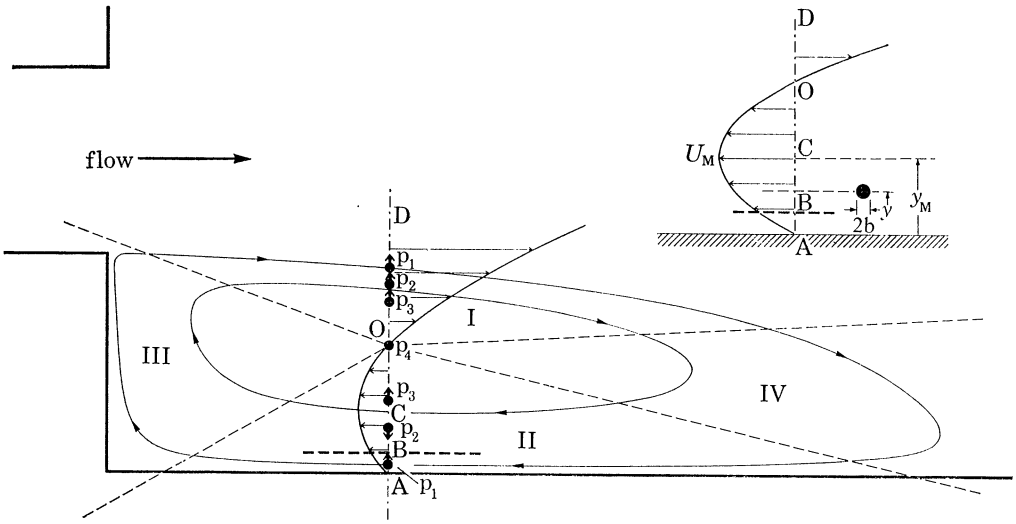

FIGURE 17. Schematic drawing of the vortex at $Re > 30$ to illustrate the radial migration of rigid spheres across the streamlines. The arrows on the particles indicate the direction of migration. Two equilibrium orbits, one close to the boundary of the vortex and the other passing through $U = U_M$, are drawn. The dashed lines divide the vortex into regions I and II where flow is roughly parallel to the tube walls and the velocity distribution is as shown, and III and IV in which flow is predominantly in the radial direction. The co-ordinates used to describe migration are shown upper right.

Applying these results to a rigid sphere circulating in the vortex, one would expect a particle initially in an orbit close to the boundary (P1 in figure 17) to migrate inward from the wall toward the equilibrium position at B while moving in the reverse flow region, but to migrate outward toward the axis in the forward flowing region. This could result in the sphere taking up an equilibrium orbit passing through a point having $y < y^*$. A particle (P2 in figure 17) initially located in a smaller orbit, $y^* < y < y_M$, would migrate outward in both regions I and II of the vortex and attain the same equilibrium orbit as the sphere P1. One can also postulate an equilibrium orbit for a particle (P3 in figure 17) initially located in an orbit, $y_M < y < 2y_M$. Such a particle would migrate outward in the forward, and inward in the reverse flow region; the equilibrium orbit would then be located inside the orbit passing through $y = y_M$. Presumably there is also an equilibrium position, for a particle situated at the very centre of the vortex.

Even in the absence of other factors, it would be hazardous to predict in detail from the above analysis the observed effects of particle size and Reynolds number on particle migration in the

vortex. True, equation (7) does predict a rapid increase in radial migration velocity with increasing particle size ($dr/dt \propto b^3$) and fluid velocity ($dr/dt \propto U_M^2$), but it is the balance between inward and outward migration rates that determines whether the particle rejoins the mainstream or circulates in a stable orbit. Moreover, the theory would not be applicable to the experiments with particles of diameters > 10 μm for which the condition ($b/y^2 \ll 1$ no longer holds true; e.g. at $Re = 37.8$, $y_M = 50$ μm. Here, by analogy with measurements in Poiseuille flow (Karnis, Goldsmith & Mason 1966) which have shown that for $b/R > 0.2$ the equilibrium position is shifted towards the tube axis as the particle radius increases, one would expect an inward shift of the equilibrium position and an increased stability of larger particles within the vortex. Nor would the theory be applicable at higher Reynolds numbers where the condition $Re_p \ll 1$ is violated.

Furthermore, there is another mechanism which may be expected to result in the inward displacement of the circulating particles within the vortex, and which would operate in regions III and IV where flow is in the radial direction. Here, because of the close proximity of the vessel walls, a sphere travelling in an outer orbit is deflected from the fluid streamline to follow a path nearer the vortex centre. If the sphere centre is initially situated on a streamline which approaches a distance $y < b$ from the vessel wall, then there is a purely mechanical wall effect of the type described by Whitmore (1959) in connection with tube entrance effects. But even for particles on streamlines closer to the vortex centre there exists a hydrodynamic wall effect which deflects a sphere centre from its original streamline. This has been demonstrated in the viscous flow of suspensions of rigid spheres and in blood behind an advancing air-liquid meniscus where there is a progressive accumulation of particles with time (Fahraeus 1929; Karnis & Mason 1967). For the rigid spheres, it was shown that particles approaching the meniscus are carried by the radial flow toward the tube wall and return on paths situated at radial distances r smaller than those of the corresponding returning fluid streamlines. The radial deflexion of the particle from the fluid streamline increases with increasing sphere diameter and with decreasing r/R of the path of approach to the meniscus.

The time spent by the particles in regions II, III and IV of the vortex while circulating in the outer orbits is relatively long compared to that spent in region I (cf. table 2). Thus, it may well be that the inward migration would predominate at all Re, and were it not for the effects of the secondary flow even the 2.6 μm diameter spheres would be able to circulate in stable equilibrium orbits at the lower Re.

Migration of the particles in pulsatile flow is even more complex and here the flow behaviour may also be affected by the existence of a static pressure gradient. Hung (1970) has given numerical solutions to a finite-difference representation of the Navier–Stokes equations for a transient laminar flow in an expansion in which the inlet pressure oscillates. The results show that there is a gradient in pressure in the radial direction across the vortex with a low pressure zone in the centre which might affect the inward migration of particles.

The characteristics of the vortex in pulsatile flow are rather similar to those of a vortex during an impulsive acceleration (Macagno & Hung 1970), and such a situation might be encountered even in steady flow if the flow were suddenly disturbed.

(*c*) *Application to blood flow*

Narrowings, or stenoses, are not uncommon in the arteries of mammals. Often, they are formed by the growth of intravascular plaques (Roach 1963; Rodbard 1966) and many of them

PHILOSOPHICAL TRANSACTIONS OF THE ROYAL SOCIETY B BIOLOGICAL SCIENCES

have an approximately axisymmetric configuration. Once formed, the subsequent development of the constriction will to some extent depend on the flow condition at, and downstream of the stenosis. It is suspected that among the effects of disturbed flow at a stenosis in an artery is the deposition of platelets and platelet aggregates in the region of flow separation (Fox & Hugh 1966; Blackshear *et al.* 1971; Goldsmith 1972). Previous work in this laboratory has shown that aggregates of 2 μm spheres serving as models of blood platelets accumulate in the low flow rate region of a vortex formed downstream of an asymmetric, one-sided spherical obstruction in a tube (Yu & Goldsmith 1973). The sudden expansion used in the present work provided an idealized model of flow downstream of an axisymmetric stenosis.

It is significant that the result obtained in the steady flow of dilute suspensions, namely that aggregates of red cells remained in the vortex while single cells and platelets migrated out into the mainstream, was shown to hold even at normal haematocrits and in pulsatile flow. The fact that the migration is in part due to the asymmetry of the expansion only makes it more probable that in the living system, the region of separated flow will be one of relatively low haematocrit. This would result in a lowered availability of oxygen for the artery wall, which it has been claimed, might lead to an increased atherogenesis (Back 1975*b*).

Another result of interest for arterial blood flow was the relatively long residence time of particles in the vortex which allowed frequent interparticle collisions to occur. Some of these, as observed with latex spheres and blood platelets, led to the formation of doublets, triplets and multiplets, which because of their larger size migrated into stable equilibrium orbits, or into the vortex centre. Recent experiments have demonstrated that when platelets are activated by exposure to low concentrations of aggregating agents such as adenosine diphosphate or thrombin prior to flow through the expansion, the aggregates, formed as a result of collisions, migrated to the centre of the vortex where they continued to grow in size until one large particle occupied almost the whole of the central region of the annulus. In pulsatile flow, however, the aggregates did not grow to such a large size, but because of the continuous influx of new platelets into the oscillating vortex a large number of smaller aggregates were formed. This work, which will be fully reported in a subsequent communication, demonstrates that the vortex does indeed provide a region in which thrombi can form and accumulate and eventually contribute to the growth of the existing stenosis.

This work was supported by the Medical Research Council of Canada (grant MT-1835) who also supported one of us (T. K.) through the award of a studentship, and by the Quebec Heart Foundation. The authors gratefully acknowledge the encouragement and advice of Dr T.-K. Hung and Dr R. G. Cox.

References

Back, L. H. 1975*a* Theoretical investigation of mass transport to arterial walls in various blood flow regions. I. Flow field and lipoprotein transport. *Math. Biosc.* **27**, 231–262.

Back, L. H. 1975*b* Theoretical investigation of mass transport to arterial walls in various blood flow regions. II. Oxygen transport and its relationship to lipoprotein accumulation. *Math. Biosci.* **27**, 263–285.

Back, L. H. & Roschke, E. J. 1972 Shear-layer flow regimes and wave instabilities and reattachment lengths downstream of an abrupt circular channel expansion. *J. appl. Mech.* **39**, 677–681.

Benis, A. M., Nossel, H. L., Aledort, L. M., Koffsky, R. M., Stevenson, J. F., Leonard, E. F., Shiang, H. & Litwak, R. S. 1975 Extracorporeal model for study of factors affecting thrombus formation. *Thromb. Diathes. Haemorrh.* **34**, 127–144.

PHILOSOPHICAL TRANSACTIONS OF THE ROYAL SOCIETY B BIOLOGICAL SCIENCES

Blackshear, P. L., Forstrom, R. J., Lorberbaum, M., Gott, V. L. & Sovilj, R. 1971 A role of flow separation and recirculation in thrombus formation on prosthetic surfaces. *AIAA 9th Aerospace Sciences Meeting*, paper 71–103. New York.

Brenner, H. 1966 Hydrodynamic resistance of particles at small Reynolds numbers. *Adv. chem. Engng* (eds T. B. Drew, J. W. Hoopes & T. Vermeulen), vol. 6, pp. 287–438. London and New York: Academic Press.

Caro, C. G., Fitz-Gerald, J. M. & Schroter, R. C. 1971 Atheroma and arterial wall shear. Observation, correlation and proposal of a shear dependent mass transfer mechanism for atherogenesis. *Proc. R. soc. Lond.* B **177**, 109–159.

Caro, C. G. & Nerem, R. M. 1973 Transport of ^{14}C-4-cholesterol between serum and wall in the perfused dog common carotid artery. *Circulation Res.* **32**, 187–205.

Christiansen, E. B., Kelsey, S. J. & Carter, T. R. 1972 Laminar tube flow through an abrupt contraction. *A.I.Ch.E. Journal* **18**, 372–380.

Cox, R. G. & Brenner, H. 1968 The lateral migration of solid particles in Poiseuille flow. I. Theory. *Chem. Engng Sci.* **23**, 147–173.

Cox, R. G. & Hsu, S. K. 1976 The lateral migration of solid particles in a laminar flow near a plane wall. *Int. J. Multiphase Flow* (in the press).

Durst, F., Melling, A. & Whitelaw, J. H. 1972 Optical anemometer measurements in recirculating flows and flames. Fluid dynamic measurements in industrial and medical environments. *Proc. DISA conf.* vol. 1, paper II, 2–2. Leicester University Press.

Durst, F., Melling, A. & Whitelaw, J. H. 1974 Low Reynolds number flow over a plane symmetric sudden expansion. *J. Fluid Mech.* **64**, 111–113.

Fahraeus, R. 1929 The suspension stability of blood. *Physiol. Rev.* **9**, 241–274.

Feuerstein, I. A., Pike, G. K. & Round, G. F. 1975 Flow in an abrupt expansion as a model for biological mass transfer experiments. *J. Biomech.* **8**, 41–51.

Forrester, J. H. & Young, D. F. 1970*a* Flow through a converging-diverging tube and its implications in occlusive vascular disease. I. Theoretical development. *J. Biomech.* **3**, 297–305.

Forrester, J. H. & Young, D. F. 1970*b* Flow through a converging-diverging tube and its implications in occlusive vascular disease. II. Theoretical and experimental results and their implications. *J. Biomech.* **3**, 307–316.

Foster, E. D. & Dobell, A. R. C. 1971 Evaluation of rigid prosthetic rings as *in vivo* intravascular thrombogenic models. *J. surg. Res.* **11**, 550–558.

Fox, J. A. & Hugh, A. E. 1966 Localization of atheroma. A theory based on boundary layer separation. *Brit. Heart J.* **28**, 388–399.

Frojmovic, M. M., Newton, M. & Goldsmith, H. L. 1976 The microrheology of mammalian platelets. Studies of rheo-optical transients and flow in tubes. *Microvasc. Res.* **11**, 203–215.

Goldsmith, H. L. 1971 Red cell motions and wall interactions in tube flow. *Fedn Proc. Fedn Am. Socs exp. Biol.* **30**, 1578–1588.

Goldsmith, H. L. 1972 The flow of model particles and blood cells and it relation to thrombogenesis. *Progress in hemostasis and thrombosis* (ed. T. H. Spaet), vol. 1, pp. 97–139. New York: Grune & Stratton.

Goldsmith, H. L. 1974 Blood flow and thrombosis. *Thromb. Diathes. Haemorrh.* **32**, 34–48.

Goldsmith, H. L., Cox, R. G. & Doubilet, G. 1977 In preparation.

Goldsmith, H. L. & Marlow, J. 1972 Flow behaviour of erythrocytes. I. Rotation and deformation in dilute suspensions. *Proc. R. Soc. Lond.* B **182**, 351–384.

Goldsmith, H. L. & Mason, S. G. 1964 The flow of suspensions through tubes. III. Collisions of small uniform spheres. *Proc. R. Soc. Lond.* A **272**, 569–591.

Goldsmith, H. L. & Mason, S. G. 1967 The microrheology of dispersions. *Rheology, theory and applications* (ed. F.R. Eirich), vol. 4, pp. 85–250. New York and London: Academic Press.

Goldsmith, H. L. & Mason, S. G. 1971 Some model experiments in hemodynamics. IV. *Theoretical and clinical* hemorheology (eds H. H. Hartert & A. L. Copley), pp. 47–59. Berlin and New York: Springer.

Goldsmith, H. L. & Mason, S. G. 1975 Some model experiments in hemodynamics. V. Microrheological techniques. *Biorheology* **12**, 181–192.

Golia, C. & Evans, N. A. 1973 Flow separation through annular constrictions in tubes. *Exp. Mech.* **13**, 157–162.

Gott, V. L., Ramos, M. D., Najjar, F. B., Allen, J. L. & Becker, K. E. 1969 The *in vivo* screening of potental thrombo resistant materials. *Artificial Heart Program Conf.* (ed. R. J. Hegyeli), p. 181. Washington, D.C.: U.S. Govt. Printing Office.

Hung, T.-K. 1970 Vortices in pulsatile flows. *Proc. Fifth Intern. Congr. Rheology* (ed. S. Onogi), vol. 2, pp. 115–127. University of Tokyo Press and University Park Press.

Hung, T.-K. & Macagno, E. O. 1966 Laminar eddies in a two-dimensional conduit expansion. *La Houille Blanche* No. 4, 391–400.

Iribarne, A., Frantisak, F., Hummel, R. L. & Smith, J. W. 1972 An experimental study of instabilities and other properties of a laminar pipe jet. *A.I.Ch.E. Journal* **18**, 689–698.

Jeffery, G. B. 1922 On the motion of ellipsoidal particles immersed in a viscous fluid. *Proc. R. Soc. Lond.* A **102**, 161–179.

PHILOSOPHICAL TRANSACTIONS OF THE ROYAL SOCIETY B BIOLOGICAL SCIENCES

Karnis, A., Goldsmith, H. L. & Mason, S. G. 1966 The flow of suspensions through tubes. V. Inertial effects. *Can. J. chem. Engng* **44**, 181–193.

Karnis, A. & Mason, S. G. 1967 The flow of suspensions through tubes. VI. Meniscus effects. *J. Colloid Interface Sci.* **23**, 120–133.

Lee, J.-S. & Fung, Y.-C. 1971 Flow in nonuniform small blood vessels. *Microvasc. Res.* **3**, 272–287.

Macagno, E. O. & Hung, T.-K. 1967 Computational and experimental study of a captive annular eddy. *J. Fluid Mech.* **28**, 43–64.

Macagno, E. O. & Hung, T.-K. 1970 Computational study of accelerated flow in a two-dimensional conduit expansion. *J. Hydraulic Res.* **8**, 41–64.

Moffat, H. K. 1964 Viscous and resistive eddies near a sharp corner. *J. Fluid Mech.* **18**, 1–18.

Morton, W. A., Parmentier, E. M. & Petschek, H. E. 1975 Study of aggregate formation in region of separated blood flow. *Thromb. Diathes. Haemorrh.* **34**, 840–854.

Packham, M. A., Rowsell, H. C., Jørgensen, L. & Mustard, J. F. 1967 Localized protein accumulation in the wall of the aorta. *Exp. molec. Pathol.* **7**, 214–232.

Roach, M. R. 1972 Poststenotic dilatations in arteries. *Cardiovascular fluid dynamics* (ed. D. H. Bergel), vol. 2, pp. 111–139. London and New York: Academic Press.

Rodbard, S. 1966 Dynamics of blood flow in stenotic vascular lesions. *Am. Heart J.* **72**, 698–704.

Segré, G. & Silberberg, A. 1962 Behaviour of macroscopic rigid spheres in Poiseuille flow. II. Experimental results and interpretation. *J. Fluid Mech.* **14**, 136–157.

Shizgal, B., Goldsmith, H. L. & Mason, S. G. 1965 The flow of suspensions through tubes. IV. Oscillatory flow of rigid spheres. *Can. J. chem. Engng* **43**, 97–101.

Smith, R. L., Blick, E. F., Coalson, J. & Stein, P. D. 1972 Thrombus production by turbulence. *J. appl. Physiol.* **32**, 261–264.

Stein, P. D. & Sabbah, H. N. 1974 Measured turbulence and its effect on thrombus formation. *Circulation Res.* **35**, 608–614.

Vasseur, P. 1973 The lateral migration of spherical particles in a fluid bounded by parallel plane walls. Ph.D. dissertation, McGill University, Montreal, Canada.

Whitmore, R. L. 1959 The viscous flow of disperse suspensions in tubes. *Rheology of disperse systems* (ed. C. C. Mill), pp. 49–59. New York and London: Pergamon Press.

Womersley, J. R. 1955 Method for the calculation of velocity, rate of flow and viscous drag in arteries when the pressure gradient is known. *J. Physiol., Lond.* **127**, 553–563.

Yu, S. K. & Goldsmith, H. L. 1973 Behavior of model particles and blood cells at spherical obstructions in tube flow. *Microvasc. Res.* **6**, 5–31.

PHILOSOPHICAL TRANSACTIONS OF THE ROYAL SOCIETY B BIOLOGICAL SCIENCES

(*a*) expansion flow

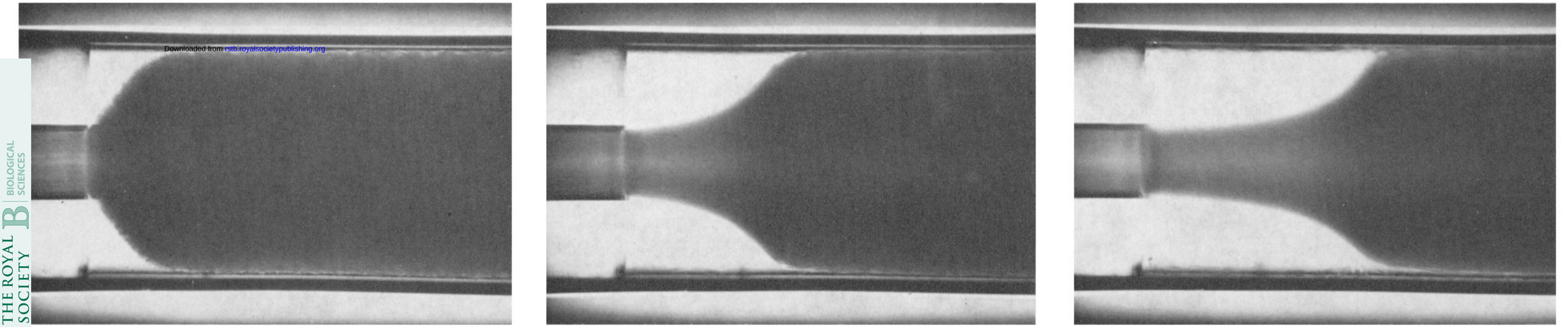

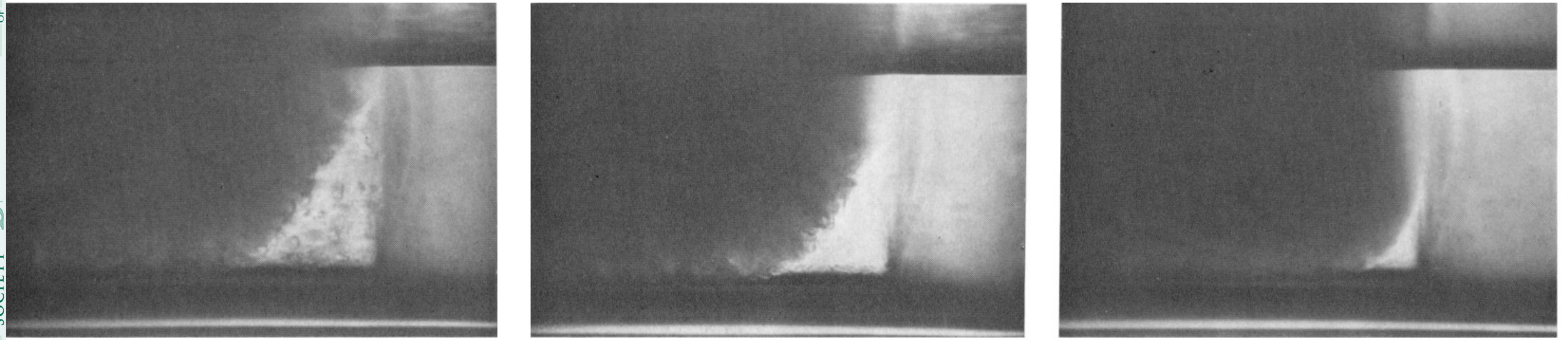

(*b*) convergent flow

FIGURE 16. Photomicrographs of a 20 % red cell suspension in steady flow through the 151–504 μm tube expansion (*a*), and in convergent flow through the same tubes (*b*). The Reynolds number increases from left to right, the values being: (*a*) 1.5, 9.0, 13.5; (*b*) 0.5, 1.5, 13.5.

PHILOSOPHICAL TRANSACTIONS OF THE ROYAL SOCIETY B BIOLOGICAL SCIENCES